BMRC RESEARCH REPORT NO. 94

DECEMBER 2003

Regional rainfall estimation using double-kriging of raingauge and satellite observations

X. Sun, M.J. Manton and E.E. Ebert

BUREAU OF METEOROLOGY RESEARCH CENTRE | AUSTRALIA

Australian Government
Bureau of Meteorology

BMRC RESEARCH REPORT NO. 94

DECEMBER 2003

Regional rainfall estimation using double-kriging of raingauge and satellite observations

X. Sun, M.J. Manton and E.E. Ebert

Australian Government
Bureau of Meteorology

BMRC
GPO Box 1289K
Melbourne VIC
Australia 3001
www.bom.gov.au

Published by the Bureau of Meteorology 2003

CONTENTS

Regional rainfall estimation using double-kriging of raingauge and satellite observations

X. Sun, M.J. Manton and E.E. Ebert

Bureau of Meteorology Research Centre
GPO Box 1289K
Melbourne, Vic., 3001 Australia

Abstract

A method for rainfall estimation combining raingauge measurements with satellite infrared data is presented. Estimates are generated in two steps: the indicator kriging (IK) technique is used first to delineate the raining areas, then ordinary kriging is used to determine the rainfall estimates in these areas. To implement IK, a binary variable is used to describe the raingauge rainfall. The satellite rainfall probability of occurrence is calculated from its infrared temperature. New methods for the merging of raingauge and satellite data and the selection of a threshold are discussed. Using a two-year period of raingauge and satellite data, the results of delineating the raining areas from indicator kriging show an improvement over the results from using raingauge data only and without indicator kriging, especially in raingauge data-sparse areas.

1. Introduction

1.1 Purpose

This report is concerned with Australian rainfall estimation, and focusses on the use of raingauge and satellite data to provide better and more effective ways of improving daily raining area delineation and spatial rainfall interpolations.

1.2 Background

Estimates of regional spatial rainfall are important for many applications. The Australian Bureau of Meteorology currently produces a daily rainfall analysis over the Australian region. A real-time grid point interpolation using the Barnes method (Mills et al., 1997 and Weymouth, et al., 1999a) is available for applications in weather and flood forecasting and the validation of numerical model output.

The primary data source in this rainfall estimation comes from the raingauge network. In Australia, a network of about 1500 stations sends telegraphic reports on a daily real-time basis. The spatial density of raingauge sites varies greatly across the country. Most of these telegraphic raingauges are located along the coastal area, while the vast inland area has less than twenty per cent of the total number of raingauges.

Other data sources for rainfall analysis, such as radar and satellite observations, arise from remote sensing. Although radar provides rainfall measurement at high spatial and temporal resolution, and has been applied in many rainfall analyses (e.g. Sun, 1998), its coverage is limited over the Australian continent. Infrared (IR) satellite imagery from geostationary satellites has been used to determine estimates of rainfall from space for nearly thirty years. The measurements of rainfall from IR satellite imagery have shown some success on monthly or weekly time scales (e.g. Arkin and Meisner, 1987, and Xie and Arkin, 1995). However, there are some serious limitations in relating satellite IR temperature to rainfall intensity or amount, especially on daily or shorter time scales.

For spatial rainfall analysis, there are a number of techniques that use statistical optimal interpolation. Daley (1991) discussed its theory and application for meteorological objective analysis. Weymouth et al. (1999b) applied statistical interpolation (SI) to rainfall estimation over the Australian region and demonstrated better performance than the Barnes method. In this report, we focus on the so-called kriging method, which is also an optimal statistical interpolation method.

Kriging has been widely used by geo-statisticians for spatial estimation. It is conceptually similar to the SI technique which has been used for rainfall estimation by Weymouth et al. (1999b). Instead of using an *a priori* first guess field of SI, an unbiased estimate condition is used in ordinary kriging. Kriging or cokriging have been used to estimate rainfall from raingauge data alone and by merging with radar data (e.g. Creutin and Obled, 1982 and Seo, 1998).

There has been little work in using satellite data in the optimal estimation process. One approach, explored by Ebert and Weymouth (1999), used a satellite no-rain threshold method in combination with gauge observations. The no-rain observations from satellites are applied to a three-pass Barnes successive-correction scheme (Achtemeier, 1987). As discussed by Weymouth (1999a),

the Barnes method is not a statistically optimised technique. Another recent result is from Grimes et al. (1999), who used kriging to incorporate satellite data in a gauge-based rainfall estimation, and demonstrated some success for estimation at a 10-day time scale.

The use of satellite infrared imagery for daily rainfall analysis is very important for at least two reasons. First, current sparse raingauge networks over central and tropical Australia do not provide the basic resolution required to describe the spatial distribution of rainfall. Secondly, rather than utilising satellite data for estimating the rainfall amount, satellite data can also be employed to estimate the rainfall occurrence; this will help to delineate rainfall areas.

1.3 Aims of the research

The specific aims of this report are to:

- analyse the spatial variability and correlation of rainfall;
- determine the potential for improved estimation by using combined raingauge and satellite data;
- apply the kriging technique for rainfall estimation, particularly for delineation of the raining area, and validate various approaches by using climate data;
- identify where further research and development are needed to improve both the theory and practice of interpolation.

This work is part of the continuing effort in BMRC to provide better real-time rainfall analysis in support of operational weather forecasting.

1.4 Scope of the research

In this report, a new approach has been developed for the delineation of rainfall. Indicator kriging is used to describe rainfall intermittency through a binary variable. This makes it possible for satellite observations of rainfall occurrence to be included in the indicator kriging to determine the rainfall area (but not the rainfall rate). The results of both raingauge and satellite data indicator kriging are effectively combined according to their error variances. The overall rainfall estimation can be subsequently determined by kriging the rainfall within the raining areas.

1.5 Structure of the report

The report is organised as follows. Section 2 discusses the issue of rainfall spatial variability and correlation. Section 3 reviews the theoretical aspects of kriging and indicator kriging for rainfall estimation. In Section 4 precipitation characteristics, including regional variations, are presented. Section 5 discusses satellite rainfall occurrence and the method of combining raingauge and satellite rain and no-rain estimates. The selection of a rain / no-rain threshold is also discussed. Section 6 describes the validation experiment and presents the results. The last section provides a summary and conclusion.

2. Analysis of rainfall spatial variability and correlation

Before we start using a variety of interpolation techniques for spatial rainfall estimation (such as kriging), the behaviour of rainfall spatial variability and correlation over the region needs to be addressed. In this section, basic spatial statistical theories that can be applied to rainfall analysis are first presented. Then, raingauge data are used for an analysis and the spatial variability of rainfall in Australia is discussed.

2.1 Measures of rainfall spatial variability and correlation

For a rainfall observation $Z(x)$ observed at point x, three second-order moments are useful in statistical analysis. They are:

(i) The variance of the variable $Z(x)$:

$$Var[Z(x)]=E\{[Z(x)-m(x)]^2\} \quad \ldots 1$$

with the first moment and expectation given by:

$$m(x)= E[Z(x)] \quad \ldots 2$$

(ii) The covariance of a variable $Z(x)$, is given by:

$$C(x_i,x_j)=E\{[Z(x_i)-m(x_i)][Z(x_j)-m(x_j)]\} \quad \ldots 3$$

where x_i and x_j are the different spatial points. As the name implies, a covariance is a measure of the spatial variation.

The covariance value for a separation distance h=0 is given by:

$$C(0)=E\{[Z(x)-m]^2\}=Var\,[Z(x)] \quad \ldots 4$$

This identifies the ordinary variance of all samples.

(iii) The correlogram is used to describe the spatial correlation relationship at different points. It can be expressed as the covariance divided by its respective variances. That is,

$$\rho(x_i, x_j) = \frac{C(x_i, x_j)}{\sqrt{Var(x_i)\cdot Var(x_j)}} \quad \ldots 5$$

The covariance and correlogram are basic statistical tools for visualising, modelling, and understanding the spatial auto-correlation of a regional variable.

2.2 Sample covariance and correlogram

The concept of second-order stationarity is needed when analysing the spatial sample covariance. The existence of second-order stationarity of a random function requires that the expectation $E[Z(x)]=m(x)$ does not depend on x in a local regime (i.e. the expectation is invariant); and the covariance depends only on the separation distance h, thus,

$$C(h)=\Sigma[Z(x)Z(x+h)]-m^2 \quad \text{for all } x \qquad \ldots 6$$

The above simplifying assumptions permit calculation of the sample covariance. Detailed discussion on these points can be found in some atmosphere objective analysis (e.g. Daley, 1991) and geostatistical books (e.g. Deutsch and Journel, 1992).

The covariance function described in Eqn 3 can be written in its sample form separated by h to $h+\Delta h$, as:

$$C(h) = \frac{1}{n(h)} \sum_{i=1}^{n(h)} z(x)z(x+h) - (m_h)(m_{+h}) \qquad \ldots 7$$

where $n(h)$ is the number of pairs separated by the distance h, z(x) is the value at the start of the pairs which can be called the *tail* value, and $z(x+h)$ is the value at the end of the pairs which can be called the *head* value. m_h and m_{+h} are given by

$$m_h = \frac{1}{n(h)} \sum_{i=1}^{n(h)} z(x) \qquad \ldots 8$$

$$m_{+h} = \frac{1}{n(h)} \sum_{i=1}^{n(h)} z(x+h) \qquad \ldots 9$$

Thus, m_h and m_{+h} are the mean of the tail and head values. Here, the random variable is traditionally denoted by capital letter Z; a random variable can take a variety of specific values (denoted by lowercase letter z) at different locations according to some probability (frequency) distribution.

If two variables Z and Y are selected, such as raingauge and satellite data, Eqn 7 can be generalised to form the sample cross-covariance $C_{zy}(h)$.

$$\rho(h) = \frac{C(h)}{\sigma_h \sigma_{+h}} \qquad \ldots 10$$

Alternatively, the sample covariance can be normalised by the respective tail and head standard deviations. This gives the rainfall correlogram:

$$\sigma^2{}_h = \frac{1}{n(h)} \sum_{i=1}^{n(h)} z(x)^2 - m^2{}_h \qquad \ldots 11$$

$$\sigma^2{}_{+h} = \frac{1}{n(h)} \sum_{i=1}^{n(h)} z(x+h)^2 - m^2{}_{+h} \qquad \ldots 12$$

where σ_h and σ_{+h} are the standard deviations of the tail and head values.

If two variables Z and Y are selected, Eqn 10 can be generalised to form the sample cross-correlogram $\rho_{zy}(h)$. $\rho(0)$ identifies the correlation coefficient between two variables at the same location.

2.3 Covariance modelling

The analysis of covariance offers a way of characterising the spatial variability of observations. Furthermore, fitting of the observed spatial covariance is needed when calculating the kriging or SI matrices. For this reason, modelling of the observed covariance is now considered.

Three models are frequently used in geostatistics. These are:

1) Gaussian model, given by

$$C(h)=C_0[exp(-h^2/3a^2)] \quad \ldots 13$$

where a is a range of covariance and C_0 is a constant.

2) Spherical model, given by

$$C(h)=C_0\,[1-(3h/2a)+(h^3/2a^3)] \quad \ldots 14$$

3) Exponential model, given by

$$C(h)=C_0\,[exp(-h/a)] \quad \ldots 15$$

In rainfall analysis, the spherical model is seldom used because its value may increase with distance. The question as to whether the Gaussian or exponential model is more appropriate to fit the rainfall spatial data will be discussed. The selection of the above modelling functions should also ensure existence and uniqueness of solutions to the kriging matrix. The additional requirement to meet these conditions is described by Journel and Huijbregts (1978).

2.4 Results of rainfall spatial variability and correlation

In order to reveal the spatial statistical characteristics of rainfall, the covariance and correlation were calculated using Eqns 7 and 10 for rainfall for each day in 1998. Pairs of raingauges are included in a separation-distance category, where the categories extend from 0 to 500 km in steps of 10 km. Both raining points and non-rain points are considered in the calculation (at least one of each pair is non-zero). Certain distance allowances must be added in the calculation. In order to allow for differences between tropical and mid-latitude rainfall systems, separate statistics are calculated north and south of 30°S. Figure 1 and Fig. 2 show the averaged covariance $C(h)$ and correlogram $\rho(h)$, respectively, for daily rainfall amounts through 1998. This gives climatological values for rainfall spatial variability and correlation. In the figures, the dashed line represents the results from the region north of latitude 30°S and the solid line south of 30°S.

Obviously, rainfall samples located next to each other are more likely to have similar values than samples located further apart. A typical covariance tends to decrease with distance h between the samples, until it reaches its minimum value. This represents the maximum range where a spatial relationship exists within the data. The correlogram equals one at the origin, then decreases with distance.

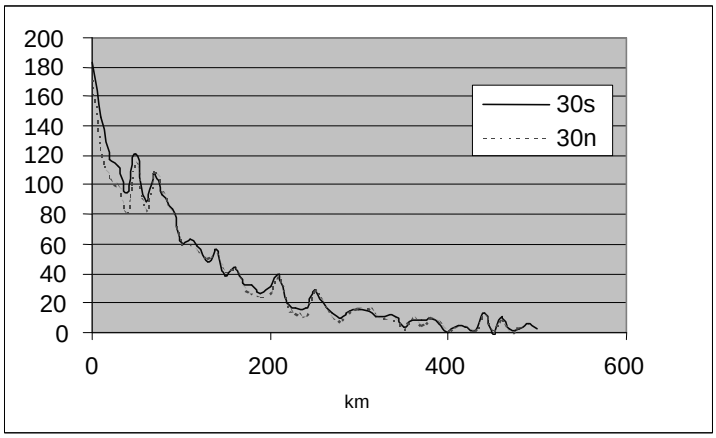

Fig. 1: Average 30°S covariance C(h) for daily rainfall amounts (mm) over the year of 1998 for the region north (30n) and south (30s) of latitude 30°S.

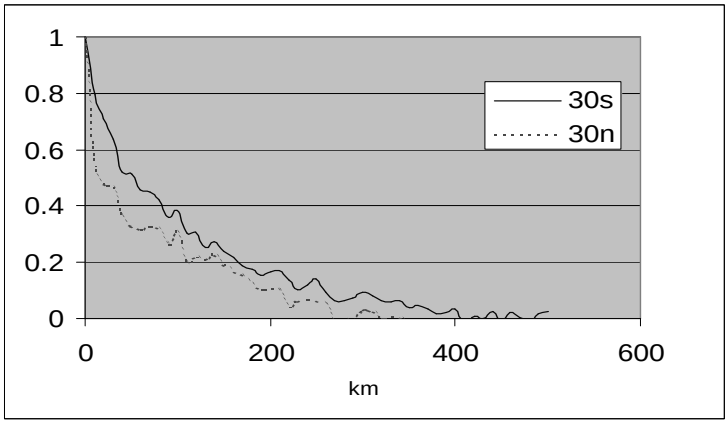

Fig. 2: Average correlogram ρ(h) for daily rainfall amounts over the year of 1998 for the region north (30n) and south (30s) of latitude 30°S.

The figures show that both the covariance and correlogram fall more sharply near the origin and reach zero at about 400 km. The figures also show the different characteristics at mid-latitudes and in the tropics (north) of Australia. The correlation in the mid-latitude region falls off more slowly than that in the tropical region. This is because a mid-latitude frontal system can produce larger-scale rainfall than tropical convective systems. A similar result was also found by Weymouth et al. (1999b), who plotted annual rainfall correlations for Australia, for different regions (separated at latitude 26°S). He found that the rainfall autocorrelation for northern Australia reached a value of 0.5 at a distance of about 35 km, compared to about 85 km in the south.

Figures 3(a) and (b) show the Gaussian and exponential models listed in section 2.3 fitted to the averaged covariance using the least-squares method. The fitted range is 500 km. The average covariance over four directions for the average of one year of data is given in the figure, which shows the fitted functions plotted as a solid line. The data fitting in the figure indicates good agreement when using both the Gaussian and exponential models (Eqns 13 and 15). The average fitting residual is 4.74 mm for the exponential, and 11.14 mm for the Gaussian model, indicating a better fit using the exponential model.

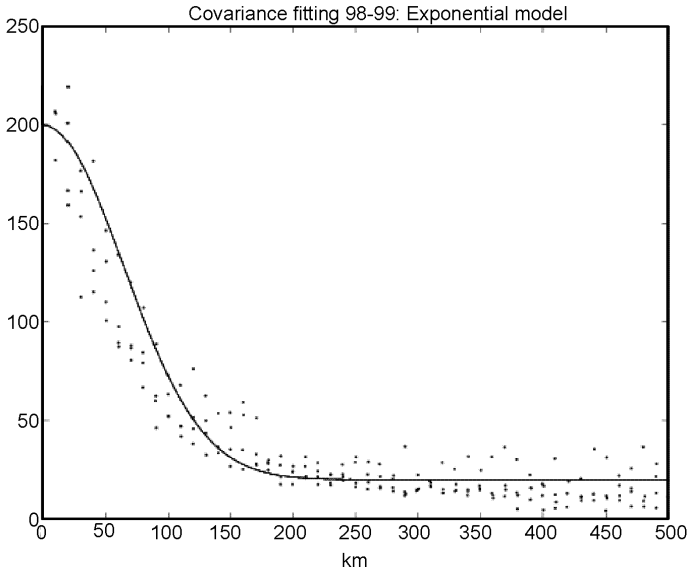

Fig. 3(a): Covariance of daily rainfall (mm) fitted by the Gaussian function.

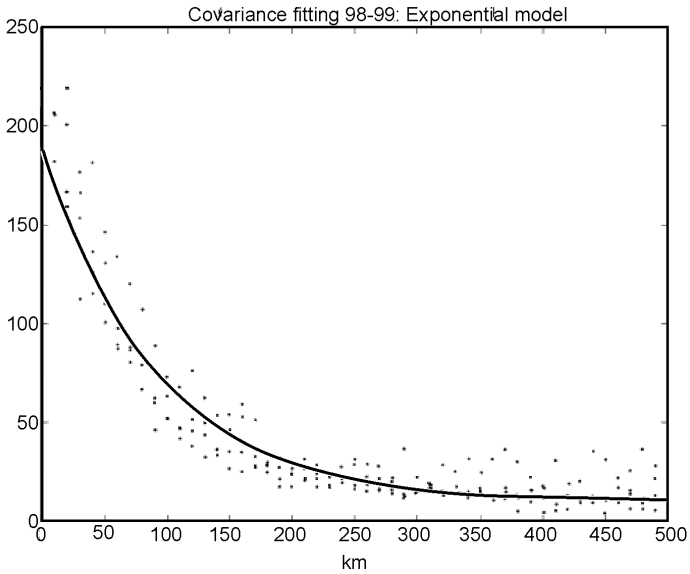

Fig. 3(b): Covariance of daily rainfall fitted (mm) by the exponential function.

On the issue of which model is considered to produce acceptable approximations of the real covariance, Krajewski (1987) and Seo et al. (1990), dealing with cokriging problems, estimated the covariance and cross-covariance functions of radar and gauge data using an exponential isotropic model. Martinez-Cob (1996) and Hevesi et al. (1992) used the Gaussian model for kriging rainfall with elevation dependence. For this study, the exponential model is adopted to fit the rainfall covariance, because the Gaussian model was sometimes too sensitive to distance and could yield unstable solutions to the kriging equation.

2.5 Indicator covariance and correlogram

Indicator kriging is used to delineate raining areas and will be discussed in detail later in this report. One of the important issues is to investigate the spatial indicator covariance and compare it to the general covariance in the previous section. Indicator covariance reflects raining or no-rain spatial correlation and variance. For calculation of the sample indicator covariance and correlogram, in Eqns 7 to 12, z is equal to one when it has rain and zero when it has no rain. Because the local indicator expectation of z equals the raining probability, the indicator covariance and correlogram measure spatial variation and correlation of rain and no-rain probability. Details of the indicator function will be discussed in Section 3.3.

Figures 4 and 5 show the averaged indicator covariance and correlogram for daily rainfall through 1998. The plots use the same data set used in Figs 1 and 2. From the figures, clearly, indicator covariance and correlogram are range-dependent. When the range equals zero, its variance is proportional to the fraction of raining areas (see further in Eqns 24-26 in section 3.3). The figures also show the same regional characteristics (i.e. differences between tropical and mid-latitude) of ordinary rainfall covariance and correlogram discussed in the previous section.

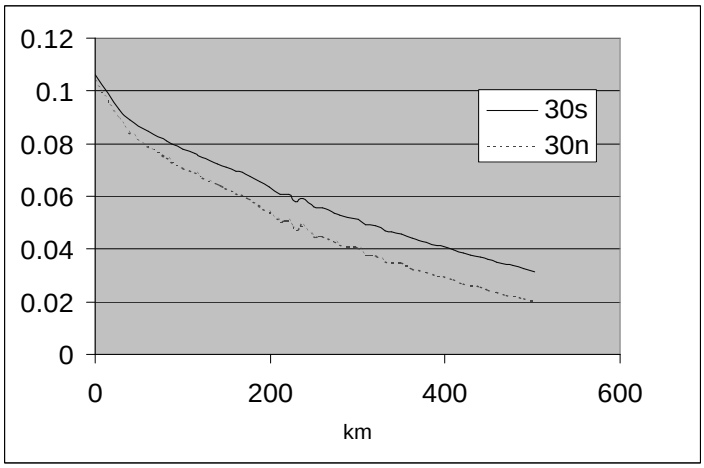

Fig. 4: Average indicator covariance for daily rainfall amounts over the year of 1998 for the region north (30n) and south (30s) of latitude 30°S.

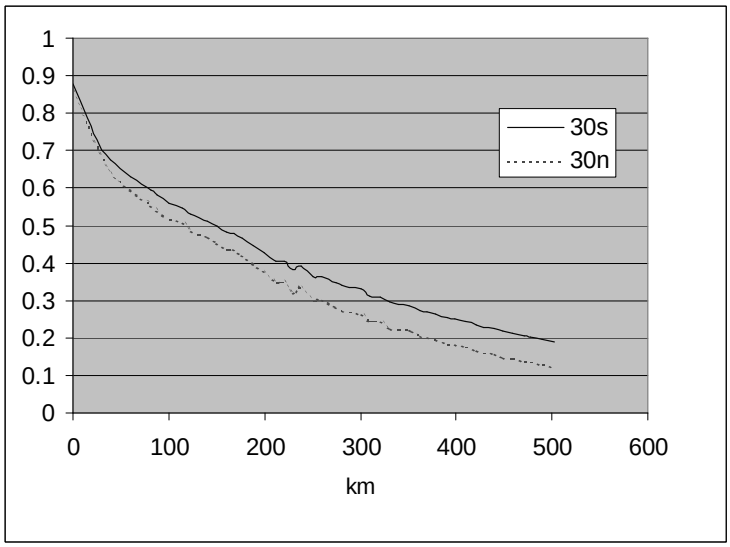

Fig. 5: Average indicator correlogram for daily rainfall amounts over the year of 1998 for the region north (30n) and south (30s) of latitude 30°S.

It is seen that both the covariance and correlation in Figs 4 and 5 do not decrease as sharply with distance as do the covariance and correlation of rainfall amount in Figs1 and 2. In other words, the rainfall indicator correlation is much higher than the correlation of rainfall itself. This could lead to improved rainfall indicator estimates.

3. Kriging and indicator kriging algorithms

3.1 Kriging

Kriging is a stochastic linear interpolation method that minimises the estimated error variances of a localised variable. The derivation of kriging equations has been discussed by many authors (e.g., Creutin and Obled, 1982; Journel and Huijbregts, 1978) and used in spatial rainfall estimation in recent years.

For a random function $Z(x)$ (in this case, rainfall at a spatial point), if the joint probability of Z_i $(i=1, n)$ has a Gaussian (normal) distribution, then its linear estimate or conditional expectation is optimal for a kriging estimate.

We consider a location x_0 with an unsampled rainfall z_0 and neighbouring rainfall observations z_i, so that its linear estimator can be expressed as:

$$E^*[Z_0|z]=E[Z_0]+\sum_{i=1}^{n} W_i(z_i-E[Z_i]) \qquad \ldots 16$$

where W_i is the kriging weight and $E[Z_0]$ is the rainfall expectation at z_0. n is the gauge number. Under the hypothesis of local stationarity of the random function Z, $E[Z_0]= E[Z_i]=m$.
The weights W_i are determined by minimising the unbiased kriging variance $E[Z_0-E^*[Z_0|z]]^2$.
That minimisation results in a set of n linear equations:

$$\sum_{i=1}^{n} W_i C(x_i, x_j) + \mu = C(x_j, x_0) \qquad \text{j=1,2,…,n} \qquad \ldots 17$$

where $C(x_i, x_j)$ are spatial covariances at different observational locations, and $C(x_j, x_0)$ are covariances between the observation and an estimated field point. μ is a Lagrange multiplier in ordinary kriging that is linked to the "unbiased" condition

$$\sum_{i=1}^{n} W_i = 1 \qquad \ldots 18$$

In Eqn 17, if $\mu = 0$, we have simple kriging, which is equivalent to the statistical interpolation (SI) method. SI is not linked to the unbiased condition but requires prior knowledge of the background field (the stationary mean m is regarded as a background field in simple kriging).

One way of estimating $E[Z_0]$ could be to use the local mean of the observed gauges, $m=\frac{1}{n}\sum_{i=1}^{n} R_i$ under stationary conditions. It is obviously inappropriate when the gauge number is low in local estimated areas. Daley (1991) suggested $E[Z_0]$ could be derived from other sources, such as numerical models. Weymouth et al. (1999b) used a Barnes interpolation field as an approximation for the background field. For simple kriging, if we do not consider the observational error to be large in the estimation process, its matrix can be related to the correlogram, rather than covariance.

In kriging, because the covariance matrix is positive definite, Eqn 17 will always have a solution. The kriging variance can then be derived as:

$$\sigma_k^2 = C(0) + \mu - \sum_{i=1}^{n} W_i C(x_i, x_0) \qquad \ldots 19$$

This is a measure of the quality of the fit to the kriging equation, rather than a measure of local estimation accuracy.

The kriging provides optimal estimation, relative to other interpolation methods, in the sense

that it minimises the least-square error for a covariance model with the unbiased condition. The weights W_i depend on the positions of observed and calculated points and the number of observations. The kriging covariances C used in this study employ an exponential model to fit the actual covariance calculated from spatial rainfall data, as described in section 2.3.

For regional rainfall estimation, kriging is performed at each estimation point using a circular search radius of 250 km. All observations that fall within this radius are included. Increasing the search radius will significantly increase the calculation burden and has only a very small impact on the estimates. The so-called moving neighbourhood search effectively uses the local stationary condition and is an effective way of dealing with the nonstationary problem over a large region.

3.2 Kriging with observation error

Rainfall data contain observation errors. These errors come from inaccurate measurement of rainfall, lack of areal representation, and the imperfect relationship between other observations (such as radar and satellite) and the rainfall. Although error bias (systematic error) can be removed through the data analysis, usually it is difficult to identify random error inherent in the data.

It is noted that the two covariances $C(x_i, x_j)$ and $C(x_i, x_0)$ in the kriging equation (Eqn 17) have different statistical representations. $C(x_i, x_j)$ is the covariance at different spatial observation stations, and it subsequently contains observation error. $C(x_j, x_0)$ is the covariance between the observational and estimation point, where the value at the estimation point should exclude observation error.

A statistical interpolation method described in Daley (1991) gives a minimised variance by proposing the concept of background and observation error covariances. The background error covariance C_b is the covariance at different locations due to the difference between the *mean* field and true field. This climate or mean field corresponds to the *mean* or expectation field m used in Section 3.1. Observation error covariance C_o represents the covariance at different locations due to the difference between the observation and true field.

According to Daley (1991), for rainfall estimation, the following assumptions should be considered. First, it is assumed that the background and observation errors are uncorrelated. Secondly, if the observation errors are regarded as uncorrelated to each other, and the observations are all made with the same type of instrument, the kriging equation can then be written as:

$$\sum_{i=1}^{n} W_i C_b(x_i, x_j) + W_i C_o(x_i, x_i) + \mu = C_b(x_j, x_0) \qquad \ldots 20$$

Compared with kriging Eqn 17, an extra term $W_i C_o$ is added to reflect the error inherent in the observational data. Equation 20 is equivalent to the statistical interpolation equation by Daley (1991) used in atmospheric objective analysis, except for the addition of the Lagrange parameter μ. Using the method explored by Daley (1991), the components of C_b and C_o can be obtained from the kriging covariance (see Appendix 1 for a detailed derivation). In our case, using the data discussed in Section 2.4, C_o is equal to 20 mm^2.

Considering observation error, the kriging estimator is no longer an exact interpolator; that is, the estimated value at an observation point does not equal the observed value, and the kriging variance is not zero at that point.

In this report, we apply the above scheme for raingauge and satellite indicator kriging as well as for raingauge rainfall estimation. The kriging estimator in the satellite indicator kriging can be used to calibrate satellite rainfall observations.

3.3 Indicator kriging

The utility of ordinary kriging for rainfall estimation is limited by particular assumptions. First, kriging provides optimal estimation only when the probability distribution is Guassian. However, for rainfall processes, rainfall is not normally distributed due to its intermittence (large numbers of zero rainfall) and few very high rainfall values. Secondly, the estimated weights and variances are independent of the data values. These assumptions may cause kriging to overestimate in the no-rain and low rainfall situations, and to underestimate in high rainfall situations.

The indicator approach is one means of overcoming both of these limitations and, therefore, of obtaining better estimates of rain areas. An indicator function is a binary variable representing zero and non-zero rainfall amounts. The departure from normality in rainfall should be greatly reduced when 'rain' and 'no-rain' are separated. A test by Hutchinson (1996) indicated the normalising power for non-zero rainfall to be between ½ to ⅓ for Australian rainfall. According to Barancourt and Creutin (1992), the transformation to a binary distribution provides a nonlinear optimal estimator. Secondly, the problem of data independence of the kriging variance is reduced since indicator kriging is conditional on the data values.

Another compelling reason for using indicator kriging is that the indicator covariance does not decrease sharply with distance and it has much greater coherence compared to rainfall covariance (discussed in Section 2). Furthermore, satellite observations provide indicator information; i.e. rainfall occurrence probability. This will be further discussed in Section 5.1.

The mathematical formulation of indicator kriging (IK) used in this report is similar to the approaches by Barancourt and Creutin (1992). First, it involves transforming the rainfall amount data into a set of binary variables. The indicator function $I(x)$ (at location x) with zero cut-off for rainfall datum value $z(x)$ may be given as:

$$I(x) = \begin{cases} =0 & Z=0 \\ =1 & Z>0 \end{cases} \qquad \ldots 21$$

Indicator kriging can be expressed in the following kriging equation:

$$E^*[I_0 \mid i] = E[I_0] + \sum_{j=1}^{n} \hat{W}_j (i_j - E[I_j]) \qquad \ldots 22$$

where $E^*[I_0|i]$ gives a spatial occurrence probability estimate, $\hat{W}_j$ is the indicator kriging weight and $E[I_0]$ is a spatial occurrence probability expectation.

With the locally homogeneous condition for kriging, we have $E[I_0]=E[I_j]= \hat{m}_j$; and $0 \le \hat{m}_j \le 1$, then

$$E^*[I_0] = \sum_{j=1}^{n} \hat{W}_j i_j + (1 - \sum_{j=1}^{n} \hat{m}_j) \qquad \ldots 23$$

The IK weight $\hat{W}_j$ can also be found by minimising the IK variance by solving Eqn 17 with the specified indicator spatial covariance.

The characteristics of IK can be described by its probability distribution. We can calculate the indicator mean as

$$\hat{m}_i = E(i(x)) = P(Z>0) \qquad \ldots 24$$

where $\hat{m}_i$ represents the cumulative probability of rainfall at x during an event. It also represents the rainfall spatial coverage, that is, raining areas.

The indicator variance can be easily derived in relation to its mean as:

$$\hat{\sigma}_i^2 = \hat{m}_i (1 - \hat{m}_i) \quad \ldots 25$$

It can be seen that, if there is no rain, then $\hat{m}_i$ =0, or if there is rain across a whole region then $\hat{m}_i$ =1, $\hat{\sigma}_i^2$ =0. When $\hat{m}_i$ =0.5, rainfall occurrence is most uncertain, and $\hat{\sigma}_i^2$ reaches its maximum value of 0.25.

With the stationary condition of the mean, the indicator covariance $\hat{C}(x_i, x_j)$ can be expressed in the form of the rainfall probability, as

$$\hat{C}(x_i, x_j) = P(Z_i>0, Z_j>0) - P(Z>0)^2 \quad \ldots 26$$

The estimated value $E^*[I_0]$ solved from indicator kriging is a conditional probability with its value lying between zero and one. Therefore, a threshold representing the dividing value needs to be selected to separate rain and no-rain estimates. This can be determined by using historical rainfall data and will be discussed in Section 5.3. Because indicator kriging, when used to delineate the rainfall area, is ultimately related to the rainfall conditional probability, it is more robust and should improve the accuracy of the rainfall estimate.

Overall, after performing indicator kriging, ordinary kriging may be subsequently used to determine the rainfall values in raining areas. Double kriging can be expressed as the product of IK and kriging, that is,

$$Z^*(x) = I^k(x)\, F^k(x) \quad \ldots 27$$

where k is a threshold, and $F^k(x)$ represents the kriging estimate over the raining area. If indicator kriging shows no rain (ie. $I^k(x)=0$), then no further estimation of $F^k(x)$ is needed.

4. Data and test field description

Australia currently has more than 6000 raingauge stations measuring daily rainfall. Of these, about 1500 telegraphic stations send daily rainfall observations in real-time. Some of these real-time stations only report when there is rain. Thus, for a particular day, only about 1000 raingauges are available for real-time access. The remaining observations are from climate raingauge stations, whose data cannot be obtained in real-time. They are usually available for analysis a month later.

Most raingauges are located near the state capital cities and there are vast areas where raingauge densities are less than 1 per 10,000 km^2. Some desert areas in central Australia have no rainfall observations. Figure 6 gives the distribution of these raingauges.

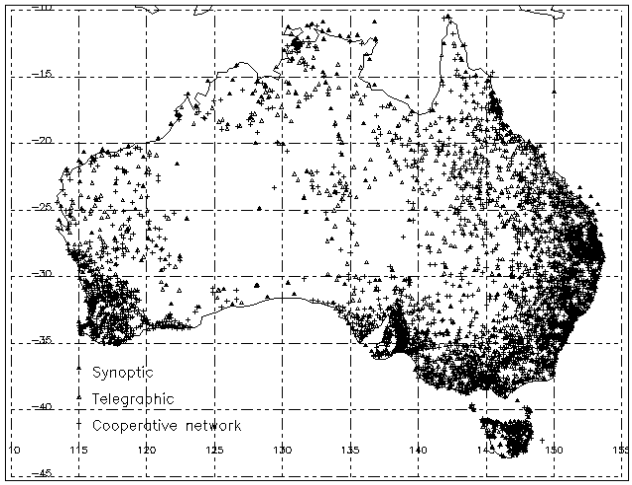

Fig. 6: Map of the Australian raingauge observation network.

We consider satellite data from the Japanese Geostationary Meteorological Satellite (GMS-5), with its infrared (IR) channel at 10.5-11.5 μm. Its spatial resolution is 5 km at nadir. The daily minimum brightness temperatures in each pixel are averaged onto a 0.25^o grid.

To verify the proposed method, an "observation" network of about 800 stations has been selected from a total of 4300 raingauge stations, representing the actual raingauge numbers used in real-time observations. These stations have been used as estimation stations to determine the estimated values for a validation network of the remaining 3500 gauge sites. The validation stations do not enter into the estimation process and are only used for validating purposes. The choice of observed and validation location is determined randomly.

It is noted that in the real-time data, some of the no-rain reports are unavailable. Therefore, the real-time data set we had to use is actually a biased data set. In the validation process, we use the unbiased climate data because real-time raingauge numbers are considered too sparse for both observation and validation. This may cause some inconsistencies. We compare their estimation differences in a later section.

Two years of daily rainfall data (1997-1998) from raingauge and satellite IR temperature are used in this analysis. Initial data quality control is performed by the operational procedures of the Australian Bureau of Meteorology.

The climate systems that affect precipitation in Australia can be crudely classified into two types divided at about 30^o latitude—tropical convective systems in the north, and mid-latitude frontal systems to the south. Most of the rainfall in the northern tropical area occurs in the summer wet season, where mainly monsoon and convective activity prevail. Southern Australia comes under the influence of rain-bearing cold fronts. Inland areas have less precipitation than those nearer the coast, particularly in winter. In summary, the rainfall pattern over Australia is expected to vary seasonally and geographically, so separating the rainfall analysis seasonally (four seasons) and geographically (at 30^oS) should be beneficial.

5. Incorporating satellite observations in indicator kriging

5.1 Satellite rain and no-rain algorithm

Many methods have been developed for the estimation of rainfall from IR satellite imagery. However, these algorithms have significant uncertainties when used for quantitative rainfall estimation, mainly due to the incorrect detection of rainfall in cold, non-precipitating cirrus clouds, and the failure to detect rain in (relatively) warm stratiform clouds. The other reason is that, for most of the time, tropical and continental cloud areas are much larger than raining areas on IR imagery. Experience with these satellite algorithms suggests that the basic premise of rainfall being associated primarily with cold cloud-top temperatures often does not hold true outside tropical regions. Ebert and Le Marshall (1995) have tested three IR algorithms over Australia; all three overestimated the rainfall amounts, with Root Mean Square (RMS) errors several times greater than the mean observed rain rate. In conclusion, IR rainfall estimates do not appear to be accurate or reliable enough to provide quantitative daily rainfall amounts to supplement the gauge observations in Australia.

Ebert and Weymouth (1999) proposed an alternative threshold method of estimating no-rain areas by identifying non-precipitating cloud or the absence of rain-bearing cloud, using the difference between the daily minimum IR brightness temperature and the climatological minimum surface temperature. Multiple thresholds were adopted by statistics according to the different climate and topography. In this report, instead of looking for a threshold that assigns no-rain values, the historical GMS IR data, together with the raingauge data, are first used to calculate rainfall probability of occurrence. The threshold used to delineate raining and no-rain areas will finally be

decided after optimal combination of the raingauge and satellite rainfall through IK estimation.

In this section, the statistical relationship between satellite temperature and rainfall frequency is explored. Similar to Ebert and Weymouth (1999) and Coakley (1988), rather than directly using average satellite brightness temperature, we use the temperature difference T_d between the daily minimum brightness temperature at each pixel and the climatological minimum daily surface temperature. These climatological minimum surface temperatures were time- and space-interpolated from 0.25^o gridded monthly average values based on 30 years of observations and processed by the National Climate Centre.

To obtain a statistical relationship between temperature difference and surface rainfall occurrence in different seasons, T_d has been matched with the frequency of raingauge rainfall R_f. R_f can be regarded as a rainfall occurrence probability at different values of T_d. It is expected that statistical information can be obtained from either low probability-of-occurrence rain (indication of no rain) or high probability-of-occurrence rain. Where the frequency equals 0.5, no useful rain or no rain information is possible.

As noted earlier, the cloud systems in northern and southern Australia differ, and so a separate statistical analysis is appropriate. Figures 7(a),(b),(c) and (d) show the rainfall frequency R_f vs. satellite T_d in four seasons for 1998, using the validation raingauge network over the Australia region. It is found that the rainfall frequency varies significantly with season and location. Although general trends are toward cold temperatures for more rainfall, the relationship between R_f and T_d is largely dependent on the broad seasonal and regional variations. In mid-latitudes, particularly in winter and spring, a T_d around –20 to –70°C corresponds to a rainfall frequency of about 50 per cent, which is much higher than in tropical areas and at summer mid-latitudes. This is due to the increase of warmer stratiform precipitation in frontal systems, and it gives an indication of the difficulty in detecting raining areas. In tropical areas, T_d could fall to –100°C or lower, with a higher frequency particularly in the wet season (November to April the following year), where convective activity prevails. In tropical areas, the relationship is close to linear.

The consistency of these results has been checked against 1997 data, and similar seasonal and regional variations were found.

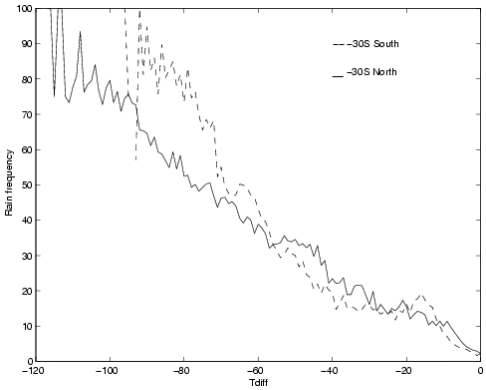

Fig. 7(a): Rainfall frequency as a function of temperature difference between daily minimum brightness temperature in each grid box and climatological minimum daily surface temperature (December 1997 - February 1998).

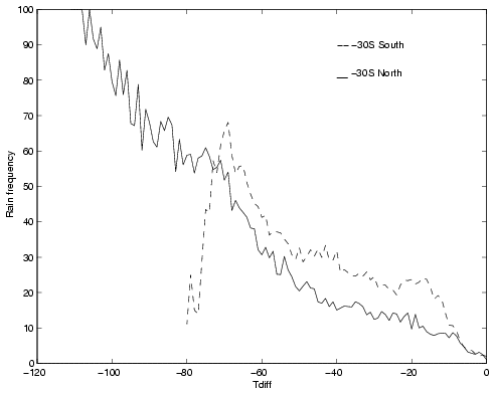

Fig. 7(b): Rainfall frequency as a function of temperature difference between daily minimum brightness temperature in each grid box and climatological minimum daily surface temperature (March - May 1998).

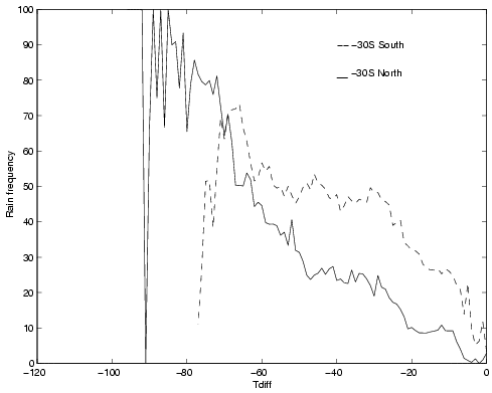

Fig. 7(c): Rainfall frequency as a function of temperature difference between daily minimum brightness temperature in each grid box and climatological minimum daily surface temperature (June - August 1998).

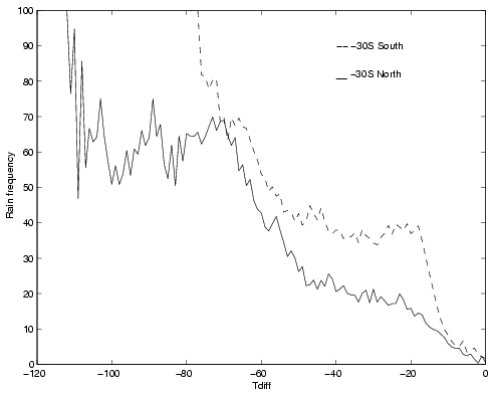

Fig. 7(d): Rainfall frequency as a function of temperature difference between daily minimum brightness temperature in each grid box and climatological minimum daily surface temperature (September - November 1998).

5.2 Merging satellite and raingauge indicator estimates

Having obtained both raingauge and satellite indicator kriging estimates, the next step is to combine the two indicator estimates with a weighting function, based on their spatial and error parameters.

In the merging of two spatial observational data sets, cokriging is considered to be capable of handling a multi-variable situation by considering both the auto-correlation of each variable and the cross-correlation among them. Some studies of using cokriging for spatial rainfall estimation can be found in Krajewski (1987) and Sun (1998). However, cokriging is computationally expensive for rainfall estimation at regional scales when a neighbourhood search scheme is applied.

A much simpler approach is used here. Conceptually similar to cokriging, Rodgers (1976), in studying the combination of satellite thermal radiation with surface temperature, used a linear optimal minimising estimate. After assuming that the error variances represent independent measurement devices, he derived a way of combining two independent measurements by taking a weighted average related to their error variances. For our applications, if the two independent measurements are raingauge and satellite rainfall indicators, the combined estimates can be expressed as:

$$I_i = \frac{\sigma_{is}^2}{\sigma_{ig}^2 + \sigma_{is}^2} I_{ig} + \frac{\sigma_{ig}^2}{\sigma_{ig}^2 + \sigma_{is}^2} I_{is} \qquad \ldots 28$$

where I_i denotes the combined indicator estimates, I_{ig} is the rainfall estimate from gauge indicator kriging and I_{is} is the rainfall estimate from satellite indicator kriging over a location, σ_{ig}^2 is the gauge indicator error variance and σ_{is}^2 is the satellite indicator error variance.

The combined error variance is

$$\sigma_i^2 = \left(\frac{1}{\sigma_{ig}^2} + \frac{1}{\sigma_{is}^2}\right)^{-1} \qquad \ldots 29$$

It can easily be proved that σ_i^2 is smaller than either σ_{ig}^2 or σ_{is}^2. Therefore, if the different observations are independent (in our case: raingauge and satellite), an appropriate combined estimate (i.e. Eqns 28-29) should reduce uncertainty even if one of the observations is less reliable; for example, an observation from a satellite.

It is noted that, rather than using the kriging variance, the error variance is used. This is because the kriging indicator variance only provides a measure of kriging indicator correlation and configuration itself, and is not directly related to the rainfall observations. Therefore, it is not a measure of data validation performance. The error variance is derived from its IK estimation and gauge validation data. It is the mathematical combination of the kriging variance and the observation error variances. On the other hand, satellite error variance arises mainly from the observations rather than the kriging method itself.

Finally, it is obvious that the number of raingauges used in the estimation has an impact on the accuracy of the kriging estimates. As a result, the error variance estimated from gauges has been related to the number of gauges used in each neighbourhood search process.

Both the error variance and kriging variance have been studied as functions of the number of raingauges. This has been shown that both variances decrease as raingauge numbers are increased. In general, the magnitude of error variance is smaller than that of the kriging variance.

Regression of the raingauge error variance against the number of raingauges N_g (see Fig. 8) is found to give:

$$\sigma^2_{ig} = -0.0015N_g + 0.157 \qquad \ldots 30$$

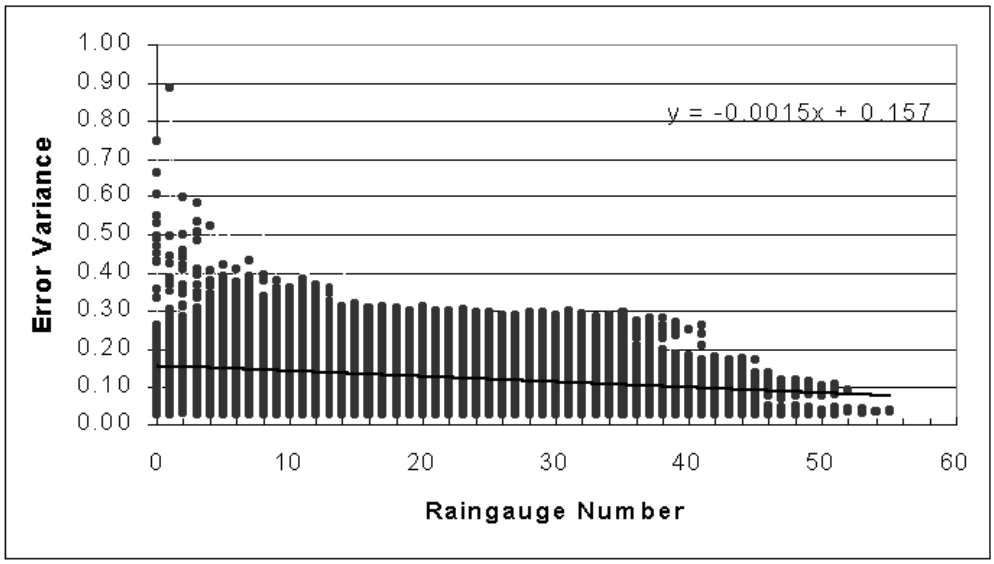

Fig. 8: Fitted relationship of error variance with raingauge number.

Satellite data are specified on a regular grid, and so the same number of grids is used in local estimation. Its average kriging error variance is constant. We allow for a geographical difference between the south and north of the Australian region. Then, we find

$$\sigma_{is}^2(x) = \begin{cases} 0.12 & \textit{tropical area (latitude >-30°)} \\ 0.15 & \textit{mid-latitude area (latitude <-30°)} \end{cases} \quad \ldots 31$$

The differences between satellite and raingauge variances give an indication that, in the case of a sparse gauge network area, satellite data have a greater weight. Thus the uncertainty in a sparse gauge network can be reduced.

5.3 Selection of rain and no-rain threshold

As the combined estimated rainfall from Section 5.2 represents rainfall occurrence probability, an appropriate threshold needs to be determined. This cut-off value (*k* in Eqn 27) is used to finally separate the raining and no-rain areas. Currently, there is no theoretical approach for the selection of the threshold. In this report, the unbiased threshold is determined by validation, using the actual rainfall estimation data set.

One way of achieving this objective is to use a contingency table and its verification parameters (Stanski et al., 1989). This approach is often used in the verification of binary variables. For the rainfall indicator validation, the category can be divided into four numbers: N1 to N4, representing different outcomes in a contingency table, as shown in Table 1.

Table 1: Rain and no rain contingency table.

	Observed no rain	Observed rain
Estimated no rain	N1	N2
Estimated rain	N3	N4

In Table 1, *N1* and *N4* represent correctly estimated numbers and *N2* and *N3* represent incorrectly estimated numbers for observed (validated) no rain and rain results respectively. From Table 1, a goodness score *S* can be defined as the number of correctly estimated minus the number of incorrectly estimated over the total number of points:

$$S = \frac{N1 + N4 - N2 - N3}{N1 + N2 + N3 + N4} \qquad \ldots 32$$

where *S* varies from -1 to1. Higher scores indicate more correct estimates.

Subsequently, biases B_1 and B_2 can be defined as the number of estimated divided by the number of observed events for no rain and rain categories.

$$B_1 = \frac{N1 + N2}{N1 + N3} \qquad \ldots 33.$$

$$B_2 = \frac{N3 + N4}{N2 + N4} \qquad \ldots 34$$

Obviously, when the bias equals one, there is no bias at all. When the bias is smaller than 1, the rain or no rain areas are underestimated, while values of bias greater than 1 imply overestimation.

In the process of selecting the optimised threshold, for each threshold value between 0 to 1, a contingency table and associated parameters have been calculated separately to test the performance of indicator kriging estimates. Values are calculated at about 3800 validating raingauge locations over the whole region.

Figures 9(a) and (b) show the goodness score S as a function of threshold for different specific situations. Two rainfall events are investigated, with one weak rainfall case (1-2 Jan 1998 when average rainfall was about 1.5 mm over the region) and one widespread rainfall case (11-12 Jan 1998 when the average rainfall was about 5 mm). With a total of about 8700 validation points calculated in Eqn 32 (sum of *N1* to *N4*), the number of correct estimates (*N1* and *N4*) increases with threshold. Meanwhile, the number of incorrect estimates (*N2* and *N3*) also starts to increase at the high threshold. S will reach a maximum value when the threshold is around 0.5 in both cases.

Figures 10(a) and (b) give the variations of B_1 and B_2 values at different thresholds for the same cases. From the figures, it appears that when the threshold is around 0.4, both B_1 and B_2 are approximately equal to one. This indicates the least biased values of B_1 and B_2 are obtained at this point. The unbiased threshold derived from B_1 and B_2 is 0.4 instead of 0.5 because the data set tends to be biased towards no rain cases.

Finally, Figs 9(c) and 10(c) give the goodness score and bias values over two-week data. They are consistent with the results shown in previous figures. The other tests also show that the best thresholds derived from the goodness score and bias value were not sensitive to the regional and seasonal variations, although the shapes in the figures of score and bias might change.

In conclusion, if the threshold is too small then we will wrongly identify some of the no-rain areas as raining areas, particularly in weak rainfall cases. If the threshold is too high we will wrongly identify some rain areas as no-rain areas, particularly in widespread rainfall cases. A balance can be reached when the optimal threshold is selected. From the results considered here, a threshold of 0.45 is chosen for our rainfall analysis.

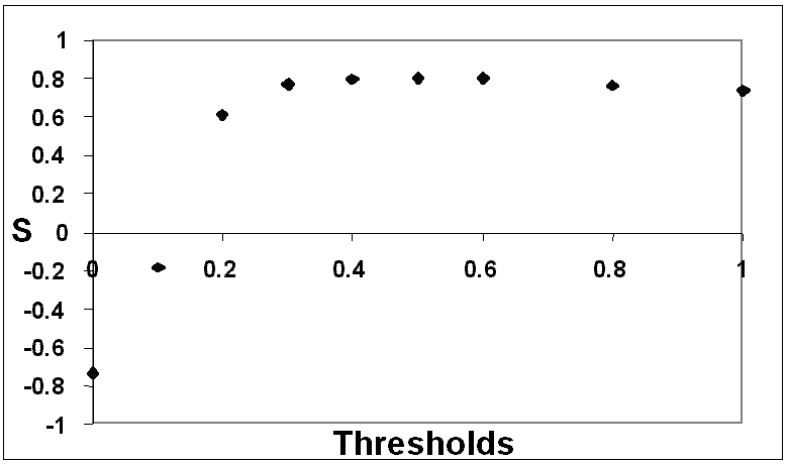

Fig. 9(a): Goodness score S at different thresholds (1-2 January 1998).

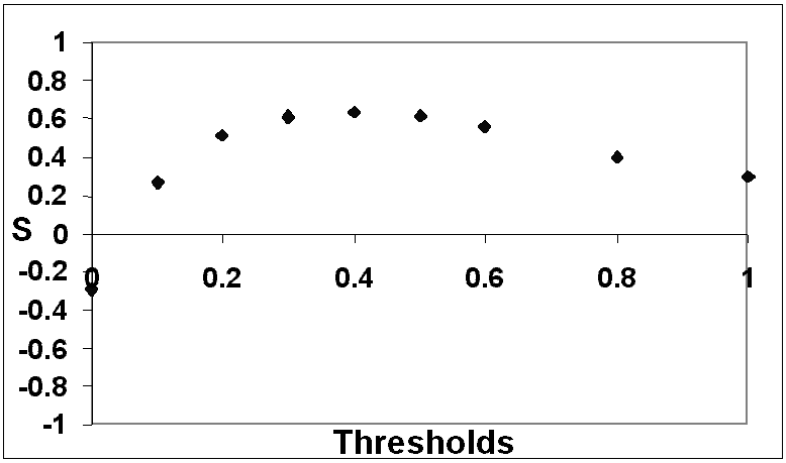

Fig. 9(b): Goodness score S at different thresholds (11-12 January 1998).

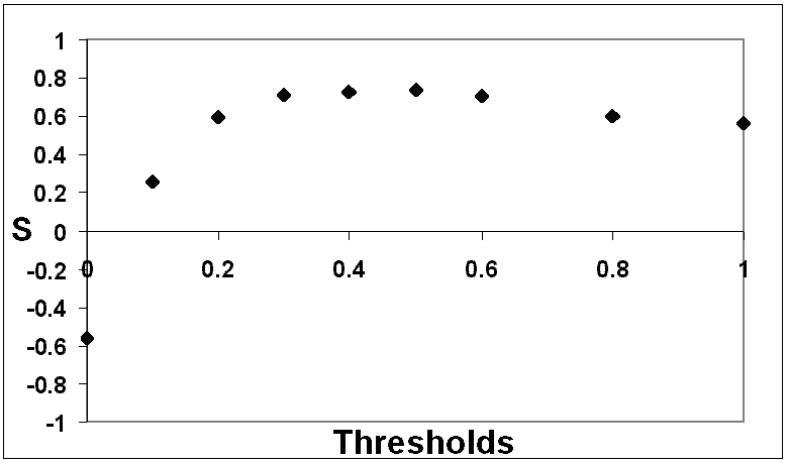

Fig. 9(c): Goodness score S at different thresholds (two weeks data, January 1998).

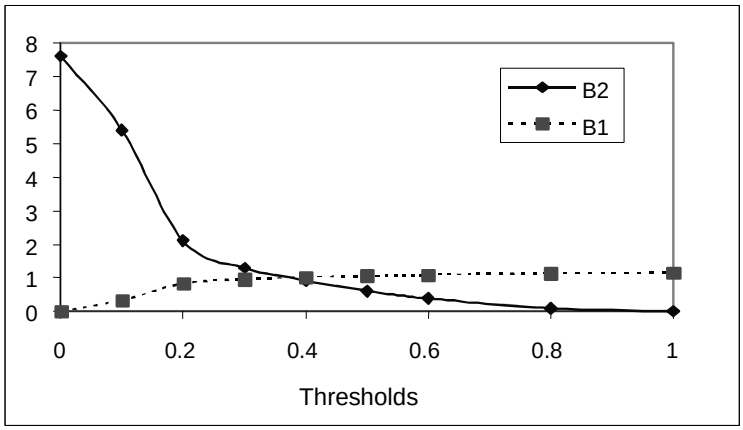

Fig. 10(a): Variations of B_1 and B_2 Bias values at different thresholds (1-2 January 1998).

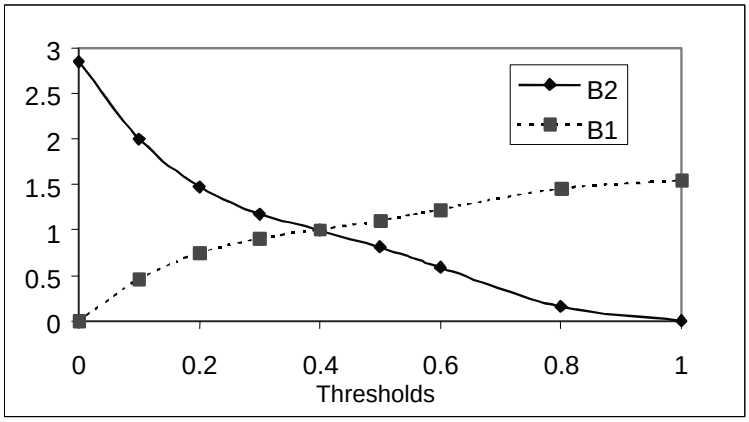

Fig. 10(b): Variations of B_1 and B_2 Bias values at different thresholds (11-12 January 1998).

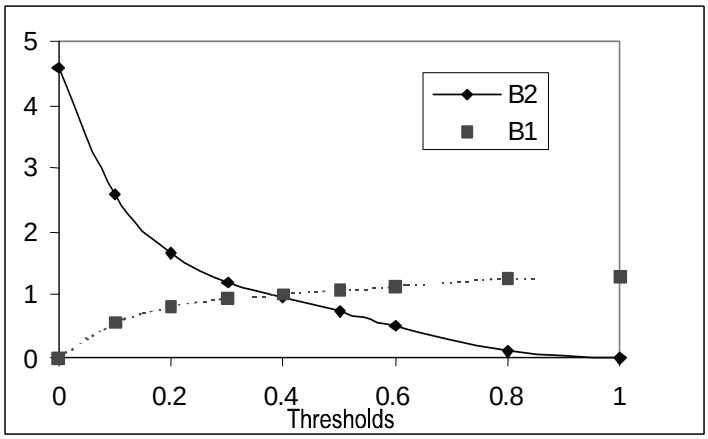

Fig. 10(c): Variations of B_1 and B_2 Bias values at different thresholds (two weeks data, January 1998).

6. Estimation results and validation

6.1 Case study

First, a typical case of daily rainfall estimation is presented; this gives a general overview of how these methods perform. Figures 11 (a)–(d) give a series of plots of daily rainfall estimates by using different methods for 25 November 1998. They are gauge kriging rainfall estimation without indicator (GK), satellite rainfall occurrence probability (SP), gauge and satellite rainfall area delineation using indicator kriging (GSIK) and gauge and satellite rainfall estimation using double kriging (GSDK). The radius of the search domain is 250 km for all the methods. In Fig. 11(a), black areas indicate no-gauge areas. For comparison, Fig. 11(e) shows all station locations of rainfall validation data (5190 raingauges from climate stations) on the same day, with symbol '+' representing sites that recorded precipitation and dots representing no precipitation. Real-time data for 1075 raingauges are used as the observational network. The estimation is carried out on a 0.25^{o} grid. In this event, due to a tropical low pressure and a subtropical front system, the rainfall was strongly convective. The measured 24-hour maximum accumulated rainfall was 109 mm for the raingauges (rainfall mean over the continent is 5.5 mm; standard deviation 12.2 mm).

Figure 11(a) shows the results of rainfall estimation performed by kriging without using IK. Compared to Fig. 11(e), it seems that the raining area derived from kriging is overestimated, mainly through falsely producing raining areas at several locations. The delineated rainfall area derived from GSIK (Fig. 11(c)) seems more realistic and is well fitted to the validation results (see Fig. 11(e)). The delineated rainfall area in Fig. 11(c) is also consistent with the occurrence probability of satellite rainfall estimation SP (Fig. 11(b)). This is important for the no-gauge data area, where the satellite may capture the rainfall area. For example, the rainfall area located around 24°S 126°E was identified by satellite data (see Fig. 11(b) and (c)), where no raingauges exist (we cannot estimate the rainfall amount). We plotted these areas as black in Fig. 11(d) to indicate a raining area.

The figures show that double kriging (GSDK – Fig. 11(d)) not only effectively combines gauge and satellite data and correctly reflects the rain and no-rain variations, but also provides optimal rainfall estimates in comparison with simple kriging methods (Fig. 11(a)). Also, the raining area is identified in the no-raingauge area.

6.2 Overall validation

To compare the overall performance of rainfall estimation techniques based on various kriging techniques, validation is carried out using Mean Absolute Error (MAE) and Root Mean Square (RMS) as indicators of performance. The functions MAE and RMS are calculated by comparing estimated rainfall with observed rainfall from validation gauge stations (average of about 3500), and we investigate the average error value over all validation gauge locations for each day and over the two-year period (1997-1998). The indicator function and rainfall estimates are calculated from observational raingauges, which are independent of the validation raingauges (see Section 4). We first look at the performance of indicator kriging using gauge indicator, satellite indicator and satellite with gauge indicator functions. Then we validate the overall performance of using kriging and double kriging on rainfall estimation.

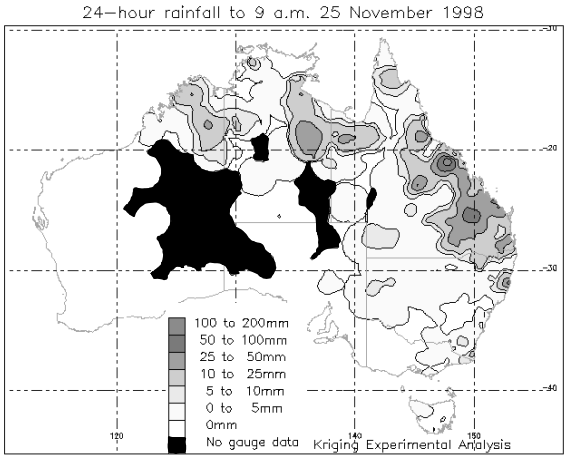

Fig. 11(a): Daily rainfall estimates using the kriging method (without indicator kriging) on 25 Nov. 1998.

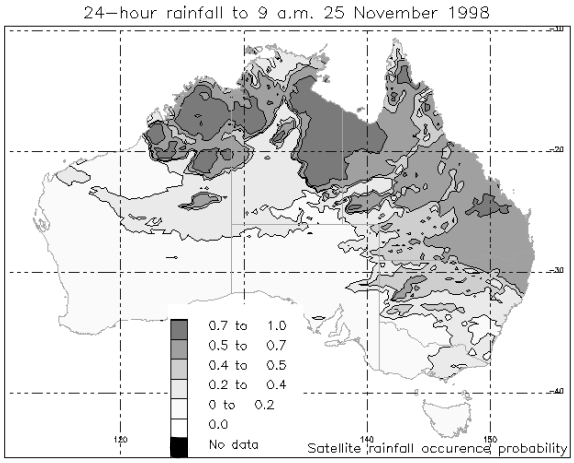

Fig. 11(b): Daily rainfall probability from satellite data on 25 Nov 1998.

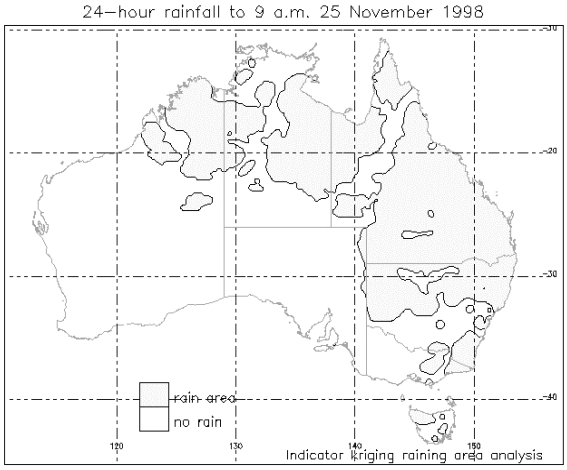

Fig. 11(c): Daily rainfall area using the indicator kriging method on 25 Nov 1998.

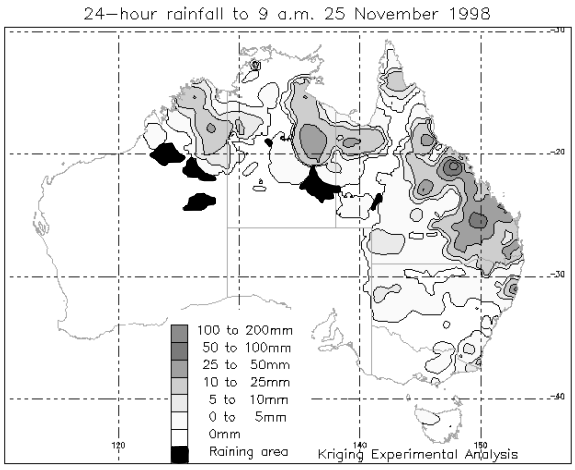

Fig. 11(d): Daily rainfall estimates using the double kriging method incorporating satellite data on 25 Nov 1998.

To check the effectiveness of using satellite data as an indicator, we validated the estimation of rain area over a sparse raingauge region in tropical and central Australia (14-32°S, 120-138°E). First, for rainfall area delineation, indicator estimates are calculated using gauge data only (GIK) and gauge data together with satellite data (GSIK). The MAE errors of GIK and GSIK are calculated for each day; in total about 670 days. The MAE error difference (i.e., GSIK-GIK) is calculated and plotted in Fig. 12 (negative values give indication of improvement by including satellite data). The horizontal coordinate gives the mean of the indicator function from validation raingauges, representing the percentage of raining gauges over total raingauges in the whole area, and its value varies from no rain (0) to the maximum raining percentage of about 62 per cent. The results show that the number of days that satellite data have improved the estimates is three times higher than the

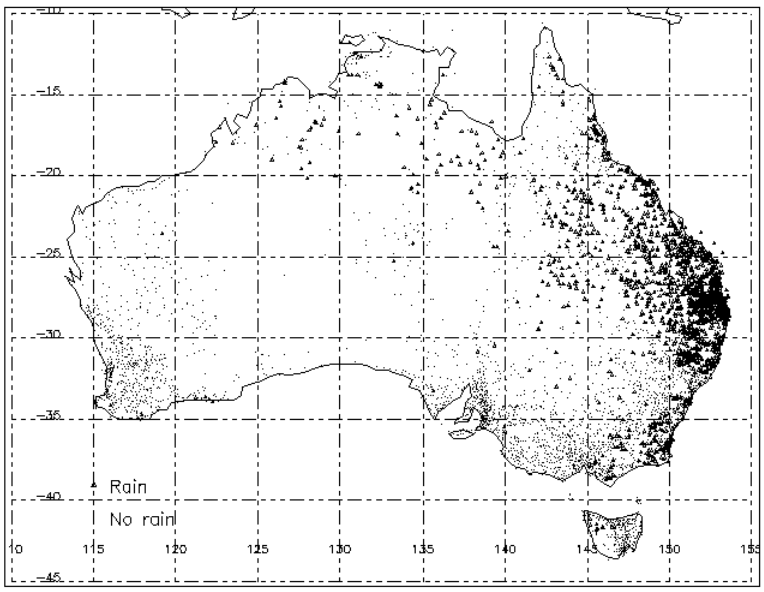

Fig. 11(e): Daily rainfall observations from validation raingauges on 25 November 1998

number of days that have worsened them. The improvement using the GSIK method is particularly significant in a widespread rainfall situation. This is because the sparse raingauge network is unable to detect rainfall in some locations. At the same time, satellite data can detect rainfall in those locations where satellite occurrence probability is high. Figure 12 also shows that even in a weak rainfall situation, the absolute error difference is small and that satellite data can still improve the estimation by detecting areas of no rain.

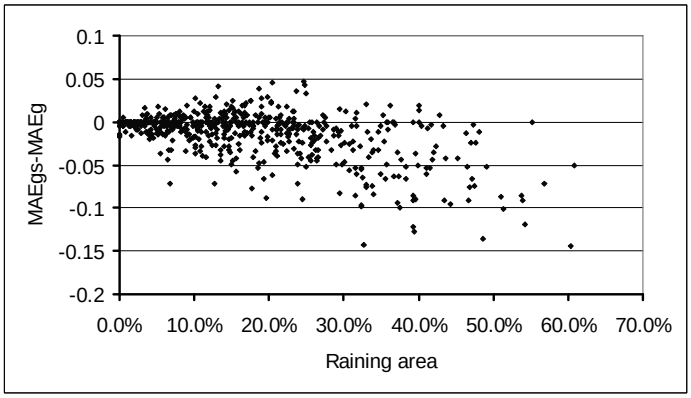

Fig. 12: Plot of MAE error differences (GSIK-GIK) on different days with different rainfall percentages.

Table 2 gives the average values of RMS and MAE for different indicator krigings in the above central and tropical gauge sparse area. They are averaged over the two-year period. Mean and standard deviation of both validated (marked as V-data Mean, V-data Std) and estimated rainfall (marked as Kriging Mean, Kriging Std). They are expressed in indicator value. Here, “no indicator kriging” means normal kriging (GK) is applied (where estimates greater than zero are regarded as raining areas).

The use of indicator kriging (both GIK and GSIK) proved to be significantly better than kriging without an indicator (GK) when estimating the raining area, because IK optimises the rain area estimates. Thus, optimal estimators are provided by improving the estimation of the non-Gaussian distribution of rainfall.

Table 2: Indicator kriging validation results for averaged daily rainfall area in central and tropical gauge sparse area.

	V-data Mean	V-data Std	Kriging Mean	Kriging Std	RMS	MAE
No indicator kriging (GK)	0.16	0.31	0.25	0.37	0.37	0.16
Gauge indicator kriging (GIK)	0.16	0.31	0.10	0.24	0.34	0.14
Satellite indicator kriging (SIK)	0.16	0.31	0.12	0.23	0.33	0.14
Gauge + sat indicator kriging (GSIK)	0.16	0.31	0.12	0.25	0.32	0.12

Similar results can be found in Table 3, where the validation over the whole Australia region is considered for these four methods. However, the differences between Table 2 and Table 3 are seen in the success of the satellite indicator, SIK, relative to the gauge-based indicator. The SIK performs better in the tropical area than it does over the whole Australian region. The satellite data itself is expected to work better in the tropical area because of its good temperature-raining relationship compared to the case for mid-latitudes. The better performance of the satellite indicator also comes from its high spatial resolution. Secondly, only small numbers of raingauges are located in the tropics. In contrast, over the south-east Australian region, the total number of raingauges is very high compared to the tropics (and could be as much as 10 times higher). Therefore, the weighting of the indicator in GSIK takes much greater account of the gauge indicator.

Table 3: Indicator kriging validation results for averaged daily rainfall area over the Australian region.

	V-data Mean	V-data Std	Kriging Mean	Kriging Std	RMS	MAE
No indicator kriging (GK)	0.25	0.41	0.45	0.47	0.50	0.25
Gauge indicator kriging (GIK)	0.25	0.41	0.24	0.40	0.37	0.14
Satellite indicator kriging (SIK)	0.25	0.41	0.11	0.21	0.46	0.21
Gauge + sat indicator kriging (GSIK)	0.25	0.41	0.24	0.40	0.36	0.13

Due to sample statistics, the validation gauge locations tend to be in regions where the overall gauge density is relatively high. Rainfall analysis is usually performed on a regular grid, and the gauge density is often sparse around many of the grid points. A test is therefore performed to study the impact of gauge density on the estimated rainfall area by gradually reducing the observed raingauge numbers. Figure 13 shows the MAE for the three methods of IK estimates as a function of raingauge number. These are average results over the two-year data set using 4000 validation

raingauges. The MAE for the satellite estimate SIK is only determined by the validation locations and is therefore constant. The figure shows that estimates from GSIK are always better than for a gauge-only method GIK, until no observational gauge exists. In that situation, the GSIK tends to the satellite estimate and GIK tends to the value where all the estimated values are zero.

Figure 13 shows that, although on average the satellite rain area estimation is relatively poor compared to the dense gauge network, it can improve the estimate in areas where there are no, or few gauges. Without satellite data, zero rainfall is assumed in regions where there are no gauges.

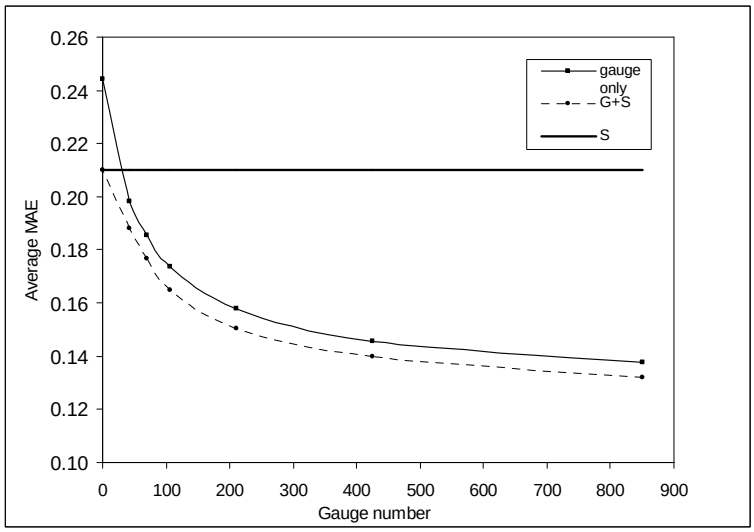

Fig. 13: MAE errors for three methods of indicator kriging estimates with different raingauge numbers.

To verify the impact of raining coverage on the performance of indicator kriging, a test is also performed for indicator kriging by separating the validation raining area into three rainfall area categories: rain area greater than 50 per cent, less than 20 per cent and between 20 and 50 per cent. The results seem consistent regarding the performance of different methods in the report. For obvious reasons, the satellite is more effective if the rain area is >50 per cent.

For rainfall estimation over the identified raining areas, the overall performance of double kriging is calculated and differences from other methods are shown in Table 4. Measured by RMSE and MAE, the gauge and satellite kriging (GSDK) performs best. However, double kriging may produce a mean bias of about 5 percent because most of the optimal estimation methods tend to underestimate the results (smoothing effect); the bias may also come from the indicator kriging where it may remove some gauge observations. Secondly, Table 4 shows that the improvement from GSDK is also marginal compared to GDK. Further tests show that GSDK has a somewhat greater impact as the number of gauges is reduced. One reason for the small impact of satellite data on actual rainfall estimates is that satellite data can only provide raining information in the indicator estimation process, but they are not used to estimate the rainfall amounts. Therefore, for the second kriging only the gauge data are involved in the raining area. In conclusion, indicator kriging does not have a great impact on rainfall amount estimations.

Further tests have also been performed by separating validations of the raining area into weak (rainfall less than 1 mm), medium (between 1 and 5 mm) and heavy rain (greater than 5 mm) categories for double kriging. Again, performance of the different methods seems consistent, except for the differences in their absolute values.

Table 4: Double kriging validation results for daily rainfall (mm) over the Australian region.

	V-data Mean	V-data Std	Kriging Mean	Kriging Std	RMS	MAE
Single no indicator kriging (GK)	2.04	6.47	2.03	5.17	4.59	1.42
Double gauge (GDK)	2.04	6.47	1.92	5.16	4.59	1.37
Double g+s (GSDK)	2.04	6.47	1.92	5.15	4.57	1.35

Finally, it is worthwhile to test the sensitivity of the number of raingauges to the kriging estimates and the impact of using the real-time daily rainfall database. First, a test is conducted to assess the impacts of different observation sets and validation sets by doubling the number of observation stations (around 1600 raingauges).

Table 5 is calculated using the increased number of observing stations. Compared to Table 4, the same conclusions regarding the performance of different methods remain valid. RMS and MAE errors in Table 5 are reduced due to the increase in the number of raingauges. V-data mean and V-data Std have changed little, indicating stable statistics. However, there is some increase in bias in the kriging mean.

Table 5: Double kriging validation results for daily rainfall (mm) over the Australian region using around 1600 gauges.

	V-data Mean	V-data Std	Kriging Mean	Kriging Std	RMS	MAE
Single no indicator kriging (GK)	2.03	6.46	1.91	5.17	4.52	1.37
DB gauge (GDK)	2.03	6.46	1.81	5.17	4.54	1.32
DB g+s (GSDK)	2.03	6.46	1.81	5.15	4.52	1.31

In the same manner, for indicator kriging, Table 6 is calculated from the increased number of stations. Compared to Table 3, again, nearly the same results can be found. Because the satellite data remains the same, the result is even more stable compared to Tables 1 and 4.

Table 6: Indicator kriging validation results for averaged daily rainfall area over the Australian region using around 1600 gauges.

	V-data Mean	V-data Std	Kriging Mean	Kriging Std	RMS	MAE
No indicator kriging (GK)	0.25	0.41	0.47	0.48	0.52	0.28
Gauge indicator kriging (GIK)	0.25	0.41	0.25	0.41	0.37	0.14
Satellite indicator kriging (SIK)	0.25	0.41	0.11	0.21	0.46	0.21
Gauge + sat indicator kriging (GSIK)	0.25	0.41	0.26	0.41	0.36	0.14

Until now, we have used the climate raingauge network for model verification. As our purpose is to establish a real-time rainfall analysis system, we therefore need to test the use of real-time data for observations while using climate data for validation. The following calculation is conducted for a three-month data period. Table 7 shows the validation results calculated from the climate stations and Table 8 is calculated from real-time observations. In general, the same conclusion regarding the performance of different methods remains valid, biases and errors decreased when using real-time data. This is because the real-time observations are biased towards higher rainfall.

Table 7: Double kriging validation results for daily rainfall (mm) over the Australian region using climate raingauges.

	V-data Mean	V-data Std	Kriging Mean	Kriging Std	RMS	MAE
Single no indicator kriging (GK)	2.42	8.01	2.42	6.20	6.09	1.94
DB gauge (GDK)	2.42	8.01	2.22	6.20	6.11	1.84
DB g+s (GSDK)	2.42	8.01	2.24	6.19	6.08	1.83

Table 8: Double kriging validation results for daily rainfall (mm) over the Australian region using real-time raingauges.

	V-data Mean	V-data Std	Kriging Mean	Kriging Std	RMS	MAE
Single no indicator kriging (GK)	2.42	8.01	2.49	6.55	5.58	1.79
DB gauge (GDK)	2.42	8.01	2.40	6.56	5.57	1.76
DB g+s (GSDK)	2.42	8.01	2.41	6.56	5.57	1.73

6.3 Comparison with SI and Barnes rainfall estimations

Since Barnes rainfall estimation is currently being used in operational analysis and statistical interpolation (SI) (developed by Weymouth et al. (1999b)) for Australian rainfall analysis, it is useful to compare the performances of the SI, Barnes and kriging techniques. As stated earlier (Section 1.2 and 3.1), the Barnes technique is a successive-correction interpolation scheme (Achtemeier, 1987) using the weighting functions. Weymouth et al. (1999a) used a three-pass Barnes analysis to estimate the daily rainfall over the Australian continent. The SI technique is structurally similar to kriging except that it requires a background field as a first guess (some references also call it simple kriging). That is, in Eqn 16, the rainfall expectation $E[Z_0]$ is replaced by a background field, and without the "unbiased" condition of Eqn 18. Therefore, the SI linear estimator can be written as (Daley, 1991):

$$f_{ai}=f_{bi}+\sum_{j=1,n} W_j\,(f_{oj}-f_{bj}) \qquad \ldots 35$$

where f_{ai} is the estimated rainfall and f_{bi} is the background rainfall at the estimation points and f_{oj} is the observed rainfall at the different observation locations.

To estimate error variance, by defining the true rainfall T and applying T in both sides of Eqn 35, the weights W_j can be determined using statistical least squares estimation by minimising the unbiased error variance $E[f_{ai}- T_i]^2$, as described in section 3.1 and by authors such as Daley (1991) and Weymouth et al.(1999b). That minimisation results in a set of N linear equations

expressed by a weight matrix.

Therefore, the solution of Eqn 35 (a detailed derivation can be seen in Daley, 1991) gives the following least-square optimal estimates expressed in matrix form as

$$W_j = B_j^T [B+O]^{-1} \quad \ldots 36$$

where B are the [$j \times j$] background and observational error covariance matrices. B_j^T is a covariance vector from the observation points to an estimated point. The superscript –1 indicates an inverse matrix and matrix O is observational error covariance.

The SI method we used here is from Weymouth et al.(1999b). The steps required for SI analysis are listed as follows:

(1) Determine suitable background fields. A problem may occur here because we do not have suitable background fields. Weymouth et al. (1999b) use three-pass Barnes estimates as a background field.

(2) Determine and fit the background field function. The function chosen in SI is:

$$C=(1+r/L)\exp(-r/L) \quad \ldots 37$$

(3) Determine observational and background error variances.

(4) Check data normality and SI parameter selection etc.

For our study, the same validation data sets were used as in the previous validation. Table 9 lists comparison results for SI, three-pass Barnes and kriging. The RMS and MAE from kriging are smaller than the results from the SI and Barnes techniques, with less mean bias. The better results from kriging may be because the first guess field is better determined in kriging than in the SI technique. Moreover, double kriging further reduces the estimated error compared to SI and Barnes, due to the influence of indicator kriging.

Table 9: SI and kriging validation results for daily rainfall (mm) over the Australian region.

	V-data Mean	V-data Std	Analysis Mean	Analysis Std	RMS	MAE
Kriging (GK)	2.04	6.47	2.03	5.17	4.59	1.42
Barnes	2.04	6.47	1.88	4.91	4.80	1.45
SI	2.04	6.47	1.70	4.80	4.75	1.43
Double Kriging (GSDK)	2.04	6.47	1.92	5.15	4.57	1.35

It should be noted that conclusions drawn from comparisons of the SI, Barnes and kriging are only valid for our case studies. Although most of the parameters in these methods are selected to be identical, there are still parameters that are dependent on their own formulation and assumption. For instance, the characteristics of the SI analysis can rely on the guess field used, and on precise formulation of the spatial correlation functions. Therefore, the superiority of kriging over SI and Barnes is relevant only to the particular circumstances of the report; it should not be interpreted as a more general conclusion.

7. Summary and conclusions

In this study, a method is presented for producing spatial daily rainfall analyses over the Australian region. The kriging method is used to implement spatial interpolation with a moving search technique over the region. The approach described here allows more effective use of satellite-based and raingauge-based observations for precipitation estimates. A particular interest is exploring the capability of delineation of the raining area. Indicator kriging provides a way of spatial interpolation in a probability sense. It is theoretically better than ordinary kriging for the purpose of delineating the raining area. For the satellite-based detection of the raining area, a statistical relationship between IR temperature and rainfall occurrence is derived. Kriging is also used to calibrate the satellite data to remove the observational bias. The optimised combination of rainfall indicator information derived from both raingauge and satellite indicator kriging gives a rainfall occurrence probability. Weights are derived from the error variances determined from a validation data set, then used to combine the gauge and satellite data occurrence probabilities, a concise and practical way of avoiding the complexity of cokriging. Using the contingency table, an unbiased threshold is determined by maximising the number of correct estimates and minimising the number of incorrect ones. After selecting an appropriate threshold, the raining area can be decided. The amount of rainfall can then be determined in the raining area by kriging of data from raingauges.

Indicator kriging gives better estimates than traditional kriging without indicator estimates for the delineation of the rain and no-rain areas. Use of satellite data in the indicator kriging improves the rain delineation, particularly in tropical areas where the raingauge network is sparse. For rainfall estimation over raining areas, although kriging improves estimates over the SI and Barnes techniques, the improvement of double kriging is marginal compared to simple kriging after using indicator kriging. This is so because, although indicator kriging can give an indication of raining areas, it is not used to estimate the rainfall amount.

Further work may involve the improvement of rainfall estimation in raining areas. Prospects for this will be further enhanced when satellite microwave sensors are considered. Experiments by Ebert and Manton (1998) indicated that rainfall rates estimated from the Special Sensor Microwave/Imager (SSM/I) had a better correlation with radar rainfall than other satellite remote sensing methods, particularly over the ocean, where raingauge data are not available. The use of SSM/I and IR satellite data could potentially improve both the rain and no-rain estimates and the rainfall amount in raining areas.

Acknowledgments. The authors would like to thank Dr Gary Weymouth, for providing his programs for rainfall statistical analysis and some graphics packages as well as for insightful discussions and assistance. The comments and suggestions by Bob Seaman are also greatly appreciated.

References

Achtemeier, G. L. 1987. On the concept of varying influence radii for a successive corrections objective analysis. *Mon. Weath. Rev.*, **115**, 1760-1771.

Arkin, P.A. and Meisner, B.N. 1987. Relationship between large-scale convective rainfall and cold cloud over the Western Hemisphere during 1982-84. *Mon. Weath. Rev.*, **115**, 51-74.

Barancourt, C. and Creutin, J.D. 1992. A method for delineating and estimating rainfall fields. *Water Resour. Res.*, **28**, 1133-1144.

Coakley, J.A. 1988. Dynamic threshold method for obtaining cloud cover from satellite imagery data. *J. Geophys. Res.*, **92** (D4), 3985-3990.

Creutin, J.D. and Obled, C. 1982. Objective analyses and mapping techniques for rainfall field: an objective comparison. *Water Resour. Res.*, **18**, 413-431.

Daley, R. 1991. *Atmospheric data analysis*. Cambridge University Press, Cambridge, 457pp.

Deutsch, C.V. and Journel, A.G. 1992. *GSLIB geostatistical software library and user's guide*. Oxford University Press, New York. 340pp.

Ebert, E.E. and Le Marshall, J. 1995. An evaluation of infrared satellite rainfall estimation techniques over Australia. *Aust. Met. Mag.*, **44,** 177-190.

Ebert, E.E. and Manton, M.J. 1998. Performance of satellite rainfall estimation algorithms during TOGA COARE. *J. Atmos. Sci.*, **55**, 1537–1557.

Ebert, E.E. and Weymouth, G.T. 1999. Incorporating satellite observations of 'No Rain' in an Australian daily rainfall analysis. *J. Appl. Meteorol.*, **38**, 44-56.

Grimes, D.I.F., Pardo-Igúzquiza, E. and Bonifacio, R. 1999. Optimal areal rainfall estimation using raingauges and satellite data. *J. Hydrology*, **222**, 93-108.

Hevesi, J.A., Istok, J.D. and Flint, A.L. 1992. Precipitation estimation in mountainous terrain using multivariate geostatistics: 1. Structure analysis. *J. Appl. Meteorol.*, **31**, 661-676.

Hutchinson, M. F. 1996. Truncated power of the normal distribution of daily rainfall. *Proceedings of the Second Australian Conference on Agricultural Meteorology*, 72-77.

Journel, A.G. and Huijbregts, C.J. 1978. *Mining Geostatistics*. Academic Press, London, 600pp.

Krajewski, W.F. 1987. Cokriging radar-rainfall and rain gauge data. *J. Geophys. Res.*, **92**, D8, 9571-9580.

Martinez-Cob, A. 1996. Multivariate geostatistical analysis of evapotranspiration and precipitation in mountainous terrain. *J. Hydrology*, **174**, 19-35.

Mills, G.A., Weymouth, G., Jones, D., Ebert, E.E., Manton, M., Lorkin, J. and Kelly, J. 1997. A national objective daily rainfall analysis system. *Bureau of Meteorology Research Centre Techniques Development Report, No 1*, 30pp.

Rodgers, C.D. 1976. Retrieval of atmospheric temperature and composition from remote measurements of thermal radiation. *Rev. Geophys. and Physics*, **14**, 609-624.

Seo, D.J., Krajewski, W.J. and Bowles, D.S. 1990. Stochastic interpolation of rainfall data from rain gages and radar using cokriging: 1. Design of experiments. *Water Resour. Res*, **26**, 469-477.

Seo, D.-J. 1998. Real-time estimation of rainfall fields using rain gauge data under fractional coverage conditions. *J. Hydrology*, **208**, 25-36.

Stanski, H.R., Wilson, L.J. and Burrows, W.R. 1989. Survey of common verification methods in meteorology. 2nd ed., *World Weather Research Technical Report No. 8*, World Meteorological Organization, 114 p.

Sun, X. 1998. Hydrological application of weather radar for catchment rainfall and flood estimation. Ph. D thesis, Monash University, 251p.

Weymouth, G., Mills, G.A., Jones, D., Ebert, E.E. and Manton, M.J. 1999a. A continental-scale daily rainfall analysis system. *Aust. Met. Mag.*, **48**, 169-179.

Weymouth, G., Manton, M.J. and Jones, D.A. 1999b. Analysis of rainfall from gauge observations - accuracy and statistical interpolation. Unpublished Technical Report available from BMRC, GPO Box 1289K Melbourne, Vic. Australia).

Xie, P. and Arkin, P.A. 1995. An intercomparison of gauge observations and satellite estimates of monthly precipitation. *J. Appl. Meteorol.*, **34**, 1143-1160.

Appendix 1

1. Derivation of kriging equation with observational equations (derivation of Eqn 20).

From kriging Eqn 16, we have

$$\sum_{i=1}^{n} W_i C(x_i, x_j) + \mu = C(x_j, x_0) \quad \ldots A.1$$

As stated in the report, $C(x_i, x_j)$ is the covariance at different spatial observation stations, and it contains observation error. $C(x_j, x_0)$ is the covariance between the observational and estimation point, where at the estimation point the estimation should exclude from observation error.

$$C(x_i, x_j)=E[(Z_i- E[Z_i])([Z_j- E[Z_j])] \quad \ldots A.2$$

A.2 can be further expressed as

$C(x_i, x_j)=E[(Z_i- E[Z_i]+ T_i-T_i)([Z_j- E[Z_j] + T_j-T_j)]$

$= E\{[(Z_i-T_i)–(E[Z_i]- T_i)][(Z_j-T_j)– (E[Z_j] -T_j)]\}$

$=E[(Z_i-T_i)(Z_j-T_j)]-E[(Z_i-T_i)(E[Z_j] -T_j)]- E[(E[Z_i] –T_i)(Z_j-T_j)]+E[(E[Z_i] –T_i) (E[Z_j] -T_j)]$ …A.3

where in (A.3) $E[(Z_i-T_i)(Z_j-T_j)]$ can be called observation error covariance;
$E[(E[Z_i] –T_i)(E[Z_j] -T_j)]$ can be called background error covariance; while $E[(Z_i-T_i)(E[Z_j] -T_j)]$ is the covariance between background error and observed error.
For the covariance between background error and observed error, one would expect it is uncorrelated for the reason that the rainfall bias has already been removed and only the random error exists (Daley, 1991), i.e.:

$$E[(Z_i-T_i)(E[Z_j] -T_j)]=0 \quad \ldots A.4$$

$$E[(E[Z_i] –T_i)(Z_j-T_j)]=0 \quad \ldots A.5$$

If the observation errors are regarded as uncorrelated to each other and only related to themselves and are all made with the same type of instrumental observation; i.e., covariance of observed error at different points equals zero, and the covariance of the observed error at the same point equals one. Then:

$$E[(Z_i-T_i)(Z_j-T_j)]= C_o \quad \ldots A.6$$

Finally;

$$C(x_i, x_j)= C_b + C_o \quad \ldots A.7$$

On the right-hand term, similar to the above, we have

$C(x_j, x_0)= E[(E[Z_i] - Z_j)([E[Z_o]-T_0)]$

$=E[(E[Z_i]–T_j - Z_j + T_j) (E[Z_0]-T_0)]$

$=E[(Z_i-T_i) (E[Z_0]-T_0)]+E[(E[Z_i]- T_j) (E[Z_0]-T_0)]$

$= E[(E[Z_i]- T_j) (E[Z_0]-T_0)]$

$= C_b$ …A.8

2. Derivation of C_b and C_o from C.

In Eqn 20, we need to obtain C_b and C_o from C.
First, assume $C=C_0^2 F(r)$, $C_o =E_0^2 F(r)$, $C_b =E_b^2 F(r)$. F(r) is a correlogram model and is described in Section 2 (Eqns 13-15).
From A.3, when the separation distance equals zero, we have

$$C_0^2 = E_o^2 + E_b^2 \quad \ldots A.9$$

From the correlogram, when the separating distance tends to zero, we have (Daley, 1991)

$$\rho(r \to 0) = \frac{E_b^2}{E_o^2 + E_b^2} \qquad \ldots A.10$$

ρ can be found by measuring the proportions at the zero distance from the calculated covariance and the covariance extrapolation from the small distances.

Therefore

$E_b^2 = \rho C_0^2$ …A.11

$E_o^2 = C_0^2 (1-\rho)$ …A.12

For more discussion on this topic, refer to Daley (1991).

Appendix 2

Flowchart of Kriging Programming

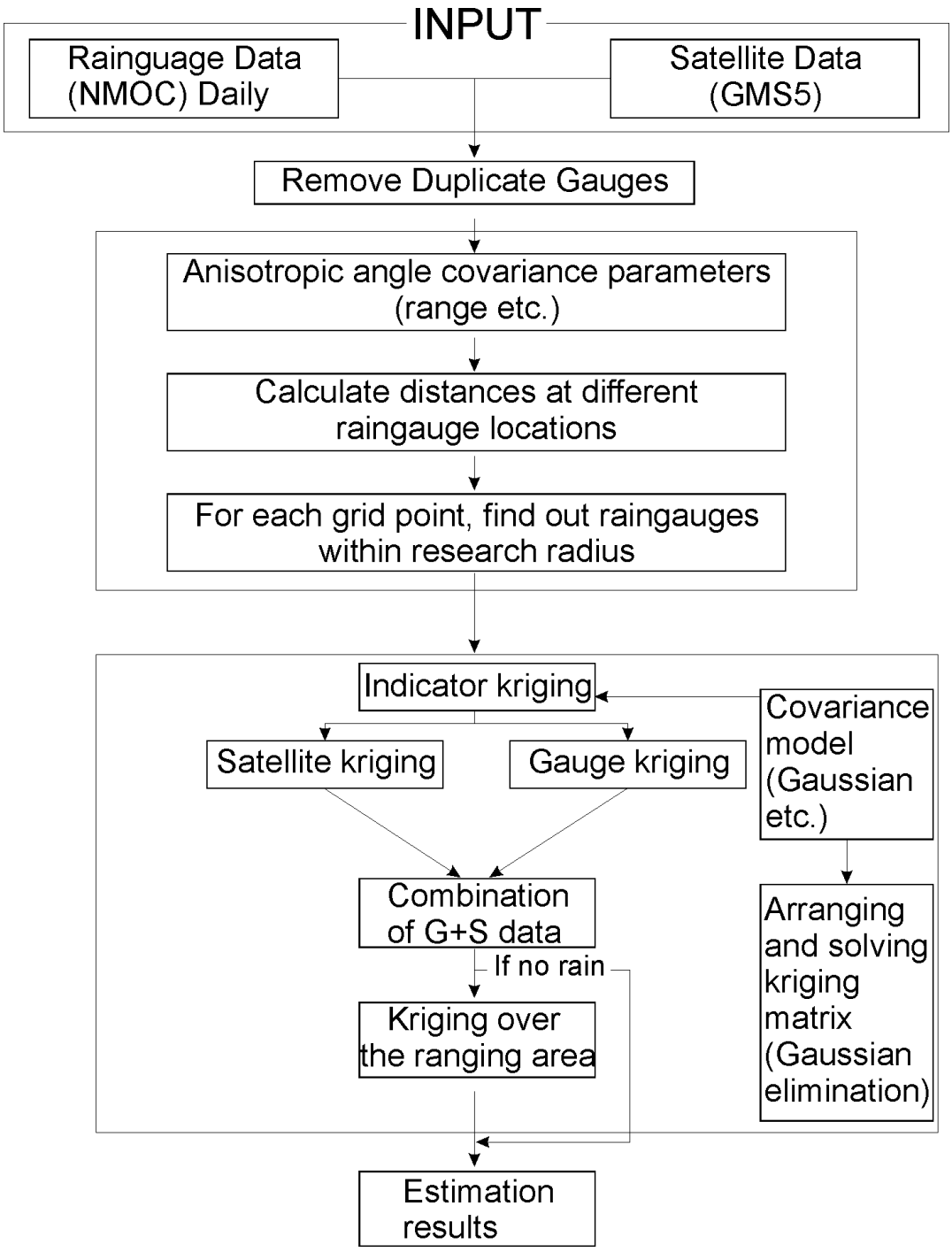

BMRC Research Reports

Holland, G.J., Berzins, I.A. and Merrill, R.T. 1985. The cyclone game: simulation of a tropical cyclone warning centre. *BMRC Research Report No. 1*, Bur. Met. Australia.

McBride, J.L. and Holland, G.J. 1986. The BMRC Australian monsoon experiment: objectives and scientific basis. *BMRC Research Report No. 2*, Bur. Met. Australia.

Spillane, K.T. and Lourensz, R.S. 1986. The hazard of horizontal windshear to aircraft operations at Sydney Airport. *BMRC Research Report No. 3*, Bur. Met. Australia.

Spillane, K.T. 1987. Convection in an inversion limited boundary layer. *BMRC Research Report No. 4*, Bur. Met. Australia.

Glowacki, T.J. and Seaman, R. 1987. A general purpose package for univariate two-dimensional data checking and analysis. *BMRC Research Report No. 5*, Bur. Met. Australia.

Williams, M. 1987. Relations between the Southern Oscillation and the troposphere over Australia. *BMRC Research Report No. 6*, Bur. Met. Australia.

Karoly, D.J., Kelly, G.A.M. and Le Marshall, J.F. 1987. The Australian Southern Hemisphere climatology data tape. *BMRC Research Report No. 7*, Bur. Met. Australia.

Keenan, T.D. and Martin, S.C. 1987. AMEX Radar Atlas. Volume 1 AMEX Phase 1. *BMRC Research Report No. 8*, Bur. Met. Australia.

Keenan, T.D. and Martin, S.C. 1987. AMEX Radar Atlas. Volume II AMEX Phase II. *BMRC Research Report No. 9*, Bur. Met. Australia.

Lajoie, F.A. 1988. Circulation asymmetries around a tropical cyclone and its future direction of motion. *BMRC Research Report No. 10*, Bur. Met., Australia.

Pike, D.J., Leslie, L.M., Mills, G.A., Glowacki, T., Hubbert, G. and McIntosh, P. 1988. Report on performance of regional forecast models January-June 1987. *BMRC Research Report No. 11*, Bur. Met. Australia.

Hart, T.L., Bourke, W.P., McAvaney, B.J., Forgan, B.W. and McGregor, J.L. 1988. Atmospheric general circulation simulations with the BMRC global spectral model: the impact of revised physical parametrisations. *BMRC Research Report No. 12*, Bur. Met. Australia.

Drosdowsky, W. 1988. Lag relations between the Southern Oscillation and the troposphere over Australia. *BMRC Research Report No. 13*, Bur. Met. Australia.

Pike, D.J., Leslie, L.M., Mills, G.A., Glowacki, T., Hubbert, G. and McIntosh, P. 1989. Report on performance of regional forecast models July-December 1987. *BMRC Research Report No.14*, Bur. Met. Australia.

Bourke, W. 1989. Working Group on Numerical Experimentation survey of model boundary condition data sets. *BMRC Research Report No. 15*, Bur. Met. Australia.

Hess, G.D. and Guymer, A.E. 1989. Verification of a Markov technique for the short-term prediction of rainfall at eight Australian stations. *BMRC Research Report No. 16*, Bur. Met. Australia.

Pike, D.J., Leslie, L.M., Mills, G.A., Glowacki, T., Hubbert, G. and McIntosh, P. 1989. Report on performance of regional forecast models January-June 1988. *BMRC Research Report No.17*, Bur. Met. Australia.

Blomley, J.E., Smith, N.R. and Meyers, G. 1989. An oceanic subsurface thermal analysis scheme. *BMRC Research Report No. 18*, Bur. Met. Australia.

Naughton, M.J. and Balgovind, R.C. 1990. BMRC Implementation of the NCAR CCM Modular Processor. *BMRC Research Report No. 19*, Bur. Met. Australia.

Hess, G.D. and Spillane, K.T. 1990. A survey of dust devils in Australia. *BMRC Research Report No. 20*, Bur. Met. Australia.

Jasper, J.D. (editor). 1990. 'The role of sea surface temperatures in numerical modelling of the atmosphere': papers presented at the first BMRC modelling workshop, July 1989. *BMRC Research Report No. 21,* Bur. Met. Australia.

Pike, D.J., Leslie, L.M., Mills, G.A., Glowacki, T., Hubbert, G. and McIntosh, P. 1990. Report on performance of regional forecast models July-December 1988. *BMRC Research Report No.22,* Bur. Met. Australia.

Pike, D.J., Leslie, L.M., Mills, G.A., Glowacki, T., Hubbert, G. and McIntosh, P. 1991. Report on performance of regional forecast models January-December 1989. *BMRC Research Report No. 23,* Bur. Met. Australia.

Colman, R.A. and McAvaney, B.J. 1991. Experiments using the BMRC general circulation model with a heat balance ocean. *BMRC Research Report No. 24,* Bur. Met. Australia.

Rikus, L. 1991. The role of clouds in global climate modelling. *BMRC Research Report No. 25,* Bur. Met. Australia.

Davidson, N.E., Puri, K., Bowen, R., Fraser, J., Wadsley, J, and Wong, H. 1991. BMRC real time analyses of the tropospheric circulation during TCM90. *BMRC Research Report No. 26,* Bur. Met. Australia.

Jasper, J.D. (editor) 1991. 'Data assimilation systems': papers presented at the second BMRC modelling workshop, September 1990. *BMRC Research Report No. 27,* Bur. Met. Australia.

Lavery, B.M., Davidson, N.E., Karoly, D.J. and McAvaney, B.J. 1991. A climatology of the western Pacific region based on the Australian tropical analysis system. *BMRC Research Report No. 28,* Bur. Met. Australia.

McAvaney, B.J., Fraser, J.R., Hart, T.L., Rikus, L.J., Bourke, W.P., Naughton, M.J. and Mullenmeister, P. 1991. Circulation statistics from a non-diurnal seasonal simulation with the BMRC atmospheric GCM: R21L9. *BMRC Research Report No. 29,* Bur. Met. Australia.

Colman, R.A., McAvaney, B.J., Fraser, J.R. and Dahni, R.R. 1992. Mixed layer ocean and thermodynamic sea ice models in the BMRC GCM. *BMRC Research Report No. 30,* Bur. Met. Australia.

May, P.T. 1992. Wind profiler measurements in the tropics. *BMRC Research Report No. 31,* Bur. Met. Australia.

Pitman, A.J., Yang, Z.-L., Cogley, J.G. and Henderson-Sellers, A. 1992. Description of bare essentials of surface transfer for the Bureau of Meteorology Research Centre AGCM. *BMRC Research Report No. 32,* Bur. Met. Australia.

Jasper, J.D. and Meighen, P.J. (eds). 1992. 'Modelling weather and climate': papers presented at the third BMRC modelling workshop, November 1991. *BMRC Research Report No. 33,* Bur. Met. Australia.

Power, S.B., Moore, A.M., Post, D.A., Smith, N.R. and Kleeman, R. 1992. On the stability of North Atlantic deep water formation in a global ocean general circulation model. *BMRC Research Report No. 34,* Bur. Met. Australia.

Power, S. and Kleeman, R. 1992. Multiple equilibria in a global ocean general circulation model. *BMRC Research Report No. 35, Bur*. Met. Australia.

Nicholls, N. 1993. Climate change and the El Niño B Southern Oscillation: report of the workshop on climate change and the El Niño B Southern Oscillation held at the Bureau of Meteorology Research Centre Melbourne, Australia 31 May and 4 June 1993. *BMRC Research Report No. 36,* Bur. Met. Australia.

Power, S.B., Colman, R.A., McAvaney, B.J., Dahni, R.R., Moore, A.M. and Smith, N.R. 1993. The BMRC coupled atmosphere/ocean/sea-ice model. *BMRC Research Report No. 37,* Bur. Met. Australia.

McAvaney, B.J. and Colman, R.A. 1993. The AMIP experiment: the BMRC AGCM configuration. *BMRC Research Report No. 38,* Bur. Met. Australia.

Jasper, J.D. and Meighen, P. J. (eds). 1993. 'Modelling severe weather': papers presented at the fourth BMRC modelling workshop, 26-29 October 1992. *BMRC Research Report No. 39,* Bur. Met. Australia.

Mullenmeister, P. and Hart, T. 1994. The UNIX verification programs. *BMRC Research Report No. 40,* Bur. Met. Australia.

Jones, D.A. 1994. A numerical vortex finding, tracking and statistics package. *BMRC Research Report No. 41,* Bur. Met. Australia.

Power, S. 1994. A report on two BMRC workshops: modelling and observing sea-ice in a coupled environment, November 19th, 1993 and physical oceanography in Melbourne, December 10th, 1993. *BMRC Research Report No. 42,* Bur. Met. Australia.

Bender, L.C. and Leslie, L.M. 1994. Evaluation of a Third Generation Ocean Wave Model for the Australian Region. *BMRC Research Report No. 43*, Bur. Met. Australia.

Keenan, T., Holland, G., Rutledge, S., Simpson, J., McBride, J., Wilson, J., Moncrieff, M., Carbone, R., Frank, W., Sanderson, B., Tapper, N. and Hallett, J. 1994. Science Plan B Maritime Continent Thunderstorm Experiment (MCTEX). *BMRC Research Report No. 44*, Bur. Met. Australia.

Pudov, V.D. and Holland, G.J. 1994. Typhoons and Ocean: results of experimental investigations. *BMRC Research Report No. 45*, Bur. Met. Australia.

Jasper, J.D. and Meighen, P.J. (eds). 1994. 'Parametrisation of physical processes': papers presented at the fifth BMRC modelling workshop, November 1993. *BMRC Research Report No. 46*, Bur. Met. Australia.

Dahni, R.R. and Stern, H. 1995. The development of a generalised UNIX version of the Victorian Regional Office's operational analogue statistics model. *BMRC Research Report No. 47*, Bur. Met. Australia.

Power, S., Kleeman, R., Colman, R. and McAvaney, B. 1995. Modelling the surface heat flux response to long-lived SST anomalies in the North Atlantic. *BMRC Research Report No. 48*, Bur. Met. Australia.

Seaman, R.S. 1995. Bias detection in the Australian sea level pressure observing network. *BMRC Research Report No. 49*, Bur. Met. Australia.

May, P.T., Holland, G.J., Keenan, T.D., Le Marshall, J.F., Colquhoun, J., Buckley, B., Love, G., Elliot, J., Dear, J. and Potts, R. 1995. Towards a comprehensive, very-short-range forecasting system for the Greater Sydney Region: observing system. *BMRC Research Report No. 50*, Bur. Met. Australia.

Sanderson, B., Tang, Y.M., Holland, G., Grimshaw, R. and Woodcock, F. 1995. A tropical cyclone maximum envelope of waters (MEOW) technique. *BMRC Research Report No. 51*, Bur. Met. Australia.

Meighen, P.J. and Jasper. J.D. (eds). 1996. 'Data assimilation in meteorology and oceanography': papers presented at the sixth annual BMRC modelling workshop, October 1994. *BMRC Research Report No. 52*, Bur. Met. Australia.

Keenan, T.D. and Manton, M.J. 1996. Darwin climate monitoring and research station: observing precipitating systems in a monsoon environment. *BMRC Research Report No. 53*, Bur. Met. Australia.

Meighen, P.J. and Jasper. J.D. (eds). 1996. 'Numerical methods': papers presented at the seventh annual BMRC modelling workshop, 4-6 December 1995. *BMRC Research Report No. 54*, Bur. Met. Australia.

Ebert. E.E. 1996. Results of the 3rd algorithm intercomparison project (AIP-3) of the global precipitation climatology project (GPCP). *BMRC Research Report No. 55*, Bur. Met. Australia.

McAvaney, B.J. and Hess, G.D. 1996. The revised surface fluxes parametrisation in BMRC: formulation. *BMRC Research Report No. 56*, Bur. Met. Australia.

Keenan, T., Puri, K., Mills, G. and Bowen, R. 1996. Regional BMRC analyses of atmospheric circulation during MCTEX. *BMRC Research Report No. 57*, Bur. Met. Australia.

Hess, G.D., McBride, J.L., Drosdowsky, W. and Whitby, F. 1996. A meteorological investigation into the Qantas flight 69 incident of severe turbulence. *BMRC Research Report No. 58*, Bur. Met. Australia.

Keenan, T.D. and Glasson, K. 1996. 'MCTEX C-band polarimetric atlas and data summary'. *BMRC Research Report No. 59*, Bur. Met. Australia.

Keenan, T.D. and Le Marshall, J. 1996. Satellite data summary and GMS imagery during MCTEX. *BMRC Research Report No. 60*, Bur. Met. Australia.

Meighen, P.J. and Jasper. J.D. (eds). 1997. 'Symposium on climate prediction and predictability': papers presented at the eighth modelling workshop, 12-14 November 1996. *BMRC Research Report No. 61*, Bur. Met. Australia.

Potts, R., Monypenny, P. and Middleton, J. 1997. An analysis of winds at Sydney Kingsford Smith airport and their impact on runway availability. *BMRC Research Report No. 62*, Bur. Met. Australia.

Sanderson, B. 1997. A barotropic ocean model for calculating storm surges. *BMRC Research Report No. 63*, Bur. Met. Australia.

Meighen, P.J. and Jasper. J.D., (eds). 1997. 'Improving short-range forecasting': abstracts of presentations at the ninth annual BMRC modelling workshop, 8-10 October 1997. *BMRC Research Report No. 64*, Bur. Met. Australia.

Drosdowsky, W. and Chambers, L. 1998. Near global sea surface temperature anomalies as predictors of Australian seasonal rainfall. *BMRC Research Report No. 65,* Bur. Met. Australia.

Power, S.B., Tseitkin, F., Colman, R.A. and Sulaiman, A. 1998. A coupled general circulation model for seasonal prediction and climate change research. *BMRC Research Report No. 66*, Bur. Met. Australia.

Power, S., Tseitkin, F., Mehta, V., Lavery, B., Torok, S. and Holbrook, N. 1998. Decadal climate variability in Australia during the 20th century. *BMRC Research Report No. 67*, Bur. Met. Australia.

Keenan, T., Kondratiev, V., Buis, B. and Christmas, R. 1998. The Bureau of Meteorology Research Centre (BMRC) portable automatic weather station: description and operation. *BMRC Research Report No. 68,* Bur. Met. Australia.

Meighen, P.J. (ed.). 1998. 'Coupled climate modelling': abstracts of presentations at the tenth BMRC modelling workshop, 12-13 October 1998. *BMRC Research Report No. 69,* Bur. Met. Australia.

Jones, D.A. 1998. The prediction of Australian land surface temperatures using near global sea surface temperature patterns. *BMRC Research Report No. 70,* Bur. Met. Australia.Tang, Y.M., Smith, N. and Greenslade, D. 1998. 'Comparison of model and observed surface winds', (report prepared for AMSA project). *BMRC Research Report No. 71,* Bur. Met. Australia.

Potts, R.J., Keenan, T. and May, P. 1999. Radar characteristics of storms in the Sydney area. *BMRC Research Report No. 72,* Bur. Met. Australia.

Greenslade, D. 1999. The assimilation of ERS-2 altimeter data into the Australian wave model. *BMRC Research Report No. 73,* Bur. Met. Australia.

Wang, Y. 1999. A triply-nested movable mesh tropical cyclone model with explicit cloud microphysics B (TCM3). *BMRC Research Report No. 74,* Bur. Met. Australia.

Jasper, J.D. and Meighen, P.J. (eds) 1999. 'Parallel computing in meteorology and oceanography': abstracts of presentations at the eleventh annual BMRC modelling workshop, 9-11 November 1999. *BMRC Research Report No. 75,* Bur. Met. Australia.

Mills, G.A. 2000. A synoptic/diagnostic study of the 1998 Sydney-Hobart yacht race storm - a warm cored extratropical cyclone. *BMRC Research Report No. 76,* Bur. Met. Australia.

Wang, G., Kleeman, R., Smith, N. and Tseitkin, F. 2000. Seasonal predictions with a coupled global ocean-atmosphere model. *BMRC Research Report No. 77,* Bur. Met. Australia.

Timbal, B. and McAvaney, B.J. 2000. A downscaling procedure for Australia. *BMRC Research Report No. 78,* Bur. Met. Australia.

Greenslade, D.J.M. 2000. Upgrades to the Bureau of Meteorology's ocean wave forecasting system. *BMRC Research Report No. 79,* Bur. Met. Australia.

Jasper, J.D. and Meighen, P.J. (eds) 2000. 'Model systematic errors': Extended abstracts of presentations at the twelfth annual BMRC modelling workshop (co-sponsored by WCRP/WGNE), 16-20 October 2000. *BMRC Research Report No. 80,* Bur. Met. Australia.

Viviand, J., Lirola, S., Timbal, B., Power, S. and Colman, R. 2000. Impact of soil moisture on climate variability and predictability. *BMRC Research Report No. 81,* Bur. Met. Australia

Mills, G.A. 2001. Impact of screen-level moisture observations in a regional data assimilation system. *BMRC Research Report No. 82,* Bur. Met. Australia.

Zhong A., Colman, R., Smith, N., Naughton, M., Rikus, L., Puri, K. and F. Tseitkin. 2001. Ten-year AMIP 1 climatologies from versions of the BMRC Atmospheric model. *BMRC Research Report No. 83,* Bur. Met. Australia.

Jasper, J.D. and Meighen, P.J. (eds) 2001. 'Understanding the climate of Australia and the Indo-Pacific region': Extended abstracts of presentations at the thirteenth annual BMRC modelling workshop, 14-16 November 2001. *BMRC Research Report No. 84,* Bur. Met. Australia.

Keenan, T., Joe, P., Wilson, J., Collier, C., Golding, B., Burgess, D., May, P., Pierce, C., Bally, J., Crook, A., Seed, A., Sills, D., Berry, L., Potts, R., Bell, I., Fox, N., Ebert, E., Eilts, M., O'Loughlin, K., Webb, R., Carbone, R., Browning,

K., Roberts, R. and Mueller, C. 2002. World Weather Research Programme forecast demonstration project: overview and current status. *BMRC Research Report No. 85*, Bur. Met. Australia.

Chambers, L., Li, F. and Nicholls, N. 2002. Seasonal climate forecasts for south-west Western Australia. *BMRC Research Report No. 86*, Bur. Met. Australia.

Voldoire, A., Timbal, B. and Power, S. 2002. Statistical-dynamical seasonal forecasting. *BMRC Research Report No. 87*, Bur. Met. Australia.

Lemus-Deschamps, L., Colman, R., Fraser, J. and Zhong, A. 2002. The model and climatological data comparison system (MACCS). *BMRC Research Report No. 88*, Bur. Met. Australia.

Zhang, H., Henderson-Sellers, A., Irannejad, P., Sharmeen, S., Phillips, T. and McGuffie, K. 2002. Land-surface modelling and climate simulations: results over the Australian region from sixteen AMIP II models. *BMRC Research Report No. 89*, Bur. Met. Australia.

Hollis, A.J. and Meighen, P.J. (eds) 2002. 'Modelling and predicting extreme events'; Extended abstracts of presentations at the fourteenth annual BMRC modelling workshop, 11-13 November 2002. *BMRC Research Report No. 90*, Bur. Met. Australia.

Wu, Z-J., Colman, R., Power, S., Wang, X. and McAvaney, B. 2002. The El Niño Southern Oscillation response in the BMRC Coupled GCM. *BMRC Research Report No. 91*, Bur. Met. Australia.

Chambers, L.E. 2003. South Australian rainfall variability and trends. *BMRC Research Report No. 92*, Bur. Met. Australia.

Meighen, P.J. and Hollis, A.J. (eds) 2003. 'Current issues in the parameterization of convection': Extended abstracts of presentations at the fifteenth annual BMRC modelling workshop, 13-16 October 2003. *BMRC Research Report No. 93*, Bur. Met. Australia.